remote sensing

MDPI

Article

Identification of Groundwater Potential Zones Using Remote Sensing and GIS Techniques: A Case Study of the Shatt Al-Arab Basin

Hadi Allafta [1,*], Christian Opp [1] and Suman Patra [2]

[1] Faculty of Geography, Philipps-University of Marburg, Deutschhausstr. 10, 35037 Marburg, Germany; opp@staff.uni-marburg.de
[2] Department of Humanities and Social Sciences, Indian Institute of Technology Kharagpur, Kharagpur 721302, West Bengal, India; suman.patra@iitkgp.ac.in
* Correspondence: Allafta@students.uni-marburg.de; Tel.: +49-17620938474

Abstract: Rapid population growth has raised the groundwater resources demand for socio-economic development in the Shatt Al-Arab basin. The sustainable management of groundwater resources requires precise quantitative evaluation, which can be achieved by applying scientific principles and modern techniques. An integrated concept has been used in the current study to identify the groundwater potential zones (GWPZs) in the Shatt Al-Arab basin using remote sensing (RS), geographic information system (GIS), and analytic hierarchy process (AHP). For this purpose, nine groundwater occurrence and movement controlling parameters (i.e., lithology, rainfall, geomorphology, slope, drainage density, soil, land use/land cover, distance to river, and lineament density) were prepared and transformed into raster data using ArcGIS software. These nine parameters (thematic layers) were allocated weights proportional to their importance. Furthermore, the hierarchical ranking was conducted using a pairwise comparison matrix of the AHP in order to estimate the final normalized weights of these layers. We used the overlay weighted sum technique to integrate the layers for the creation of the GWPZs map of the study area. The map has been categorized into five zones (viz., very good, good, moderate, poor, and very poor) representing 4, 51, 35, 9, and 1% of the study area, respectively. Finally, for assessing the effectiveness of the model, the GWPZs map was validated using depth to groundwater data for 99 wells distributed over the basin. The validation results confirm that the applied approach provides significantly solid results that can help in perspective planning and sustainable utilization of the groundwater resources in this water-stressed region.

Keywords: groundwater potential zone; analytic hierarchy process; water-stressed region; sustainable management; Shatt Al-Arab basin

Citation: Allafta, H.; Opp, C.; Patra, S. Identification of Groundwater Potential Zones Using Remote Sensing and GIS Techniques: A Case Study of the Shatt Al-Arab Basin. *Remote Sens.* **2021**, *13*, 112. https://doi.org/10.3390/rs13010112

Received: 9 November 2020
Accepted: 27 December 2020
Published: 31 December 2020

1. Introduction

Surface water is generally scant in arid and semi-arid regions owing to low rainfall and high evaporation dominated in such regions [1]. Arid and semi-arid climatic environments are undergoing a growing surface water deficit across the world [2–4]. Hence, groundwater is considered as a major alternative viable resource in these environments [5,6]. The Middle East, an arid to semi-arid region, is the most water-scarce zone in the world, with most of its countries falling under the international water poverty index set by the United Nations [7]. Among the Middle Eastern countries, Iraq and Iran are specifically facing considerable water shortages across most parts of their territories. A growing population (Table 1), increasing basin development (e.g., dam projects by riparian countries), and climate-related hazards have ultimately resulted in decreasing surface water supplies in these countries [8,9]. Presently, to safeguard the water resources in Iraq, the government has established a comprehensive groundwater monitoring program intending to improve the national scope in terms of exploration and management of the national groundwater

resources. Initiated in 2013, the program has conveyed considerable data, knowledge, and management information tools related to the groundwater resources in Iraq [10]. Similarly, in Iran where groundwater withdrawal represents around 60% of water usage (Water Uses in Iran), a number of laws have been developed to control the negative consequences of the exploitation of groundwater such as the Groundwater Resources Preservation Act, the Manner of Water Nationalization, and the Water Law. For example, the "Prohibited Plain Act" outlined in these laws defines several hydrological equations to orient the planners in the legislation of well-digging policies [11]. The Prohibited Plain Act became the milestone of consecutive regulatory laws such as banning well construction to control groundwater over-exploitation [11].

Table 1. Present and future prospective population number (in million) in Iraq, Iran, and Germany *.

	Country		
	Iraq	**Iran**	**Germany**
Mid 2019	39.3	83.9	83.1
2035	55.3	100.6	82.2
2050	70.9	113.3	79.2
Population number per square kilometer cultivable land	786	571	706

* Source: https://www.dsw.org/laenderdatenbank/.

The Shatt Al-Arab basin, a trans-boundary basin shared by Iraq and Iran, is situated in an arid water-scarce zone. The water scarcity in this basin is exacerbated by anthropogenic activities [12]. The rising burden of pollutants that the river receives from the urbanized areas [13], oil production fields [14], and agricultural areas [15] have caused deterioration in the river's water quality [16,17]. Furthermore, the Mesopotamian marshes flowing into the river that were historically serving as natural filters for contaminants [18] are no longer so due to the drainage and exsiccation during the 1990s [19,20]. Moreover, dam projects by upstream countries have reduced the water flow to the Shatt Al-Arab. Many studies have documented a drastic decline in the river discharge and increasing levels of salinity in the river due to seawater intrusion [12,21]. Therefore, the essential role that the river plays in supporting holistic communities is highly affected [22]. The surface water shortage in this basin is raising the significance of groundwater as an alternative water source [23,24]. Groundwater, however, faces a serious resource-depletion threat in this region [25,26]. For example, [27] found that during the period from 2003 to 2009, groundwater exploitation significantly increased in Iraq owing to drought and surface water shortages in the area. Groundwater resources depletion in the Shatt Al-Arab basin emphasizes the need for sustainable management of such resources to secure steady supplies of quality water. Delineation of groundwater potential zones is considered a primary step towards sustainable management of these resources [28]. However, no single recharge study has been done over the Shatt Al-Arab basin despite its regional significance as a trans-boundary basin in a water-scarce region. Therefore, investigating the groundwater potential zones in the Shatt Al-Arab basin can play a significant role in the implementation of efficient groundwater management and protection policies [29].

Groundwater is a hidden natural resource and cannot be directly detected, therefore, mapping of this resource can be a challenging task. Depiction of groundwater potential zones (GWPZs) is necessary for the optimal usage of available water resources to meet the needs of the communities [30]. Stratigraphy analyses and test drilling are the traditional and effective techniques for identifying the locations of an aquifer, but these processes are cost and time-consuming. Integration of remote sensing data in the geographical information system surroundings represents an effective alternative for the identification of GWPZs [31]. Remote sensing offers a repetitive coverage of an area in a systematic, synoptic, fast, and low-cost way with a combination of different ranges of the electromagnetic spectrum radiated from various earth features [32]. Remote sensing (RS) represents an exclusive and powerful tool for obtaining spatiotemporal data of sizable areas in a short period of time

based on indirect analyses of some directly observable terrain features. Application of RS in hydrogeological investigation and monitoring can provide significant information in spatial and temporal scales, which is important for effective analysis, prediction, and validation of water resources models [33]. The ability of satellite imagery to cover large spatial scales is essential for the depiction of basins physiographic characteristics, such as land use/land cover, slope, and drainage density as well as structural characteristics such as fractures, faults, and cleavages [34–39]. Such characteristics are major requirements for groundwater resources evaluation and exploration and were used by many researchers (e.g., Table 2) for GWPZs delineation. Geographic information system (GIS), on the other hand, provides a distinguished work environment for efficiently processing and storing geo-referenced data compiled from various sources such as satellite imagery, maps, and land surveys [40]. RS and GIS capabilities of collecting and manipulating data covering large scales within a short time represent handy tools in demarcating, assessing, and conserving groundwater resources. With such capabilities, many databases can be integrated to generate conceptual models for the identification of GWPZs of an area [41–48].

Table 2. Literature review of the thematic layers used to delineate groundwater potential zones (GWPZs).

Literature	Lt	Ge	So	DEM	Rf	Sl	LD	DD	LU	DR	WT
[49]	✓	✓					✓	✓	✓		
[50]	✓	✓	✓			✓		✓			
[51]	✓		✓		✓	✓	✓	✓	✓		
[52]	✓	✓	✓	✓		✓	✓	✓	✓		
[53]	✓	✓	✓		✓	✓	✓	✓	✓		
[54]	✓	✓	✓	✓	✓	✓	✓	✓			
[55]	✓	✓	✓		✓	✓	✓	✓	✓		
[56]	✓	✓	✓		✓	✓	✓	✓			
[57]	✓		✓		✓	✓	✓	✓	✓		
[58]	✓		✓			✓	✓	✓	✓		
[59]	✓	✓	✓		✓	✓	✓	✓	✓		
[60]	✓					✓	✓	✓	✓		
[61]	✓	✓	✓	✓	✓	✓	✓	✓	✓	✓	
[62]	✓		✓	✓	✓	✓	✓	✓	✓		
[63]	✓		✓		✓	✓	✓		✓		✓
[64]	✓	✓	✓		✓	✓	✓	✓			
[65]	✓	✓	✓		✓	✓	✓	✓	✓		
[66]	✓		✓		✓	✓	✓	✓	✓		
[67]	✓	✓	✓	✓	✓	✓		✓	✓		✓
[68]	✓	✓	✓		✓	✓	✓	✓	✓		
[69]	✓			✓			✓	✓	✓	✓	
[30]	✓	✓	✓		✓	✓	✓	✓	✓		
[70]	✓	✓	✓		✓	✓	✓	✓	✓		
[71]	✓	✓	✓		✓	✓	✓	✓	✓		✓
[72]		✓	✓	✓	✓			✓	✓		
[73]	✓					✓	✓	✓		✓	
[74]	✓	✓	✓		✓	✓	✓	✓	✓		
[75]		✓	✓		✓	✓	✓	✓	✓		
[76]	✓	✓	✓			✓	✓	✓	✓		

Lt = lithology; Ge = geomorphology; So = soil; DEM = digital elevation model; Rf = rainfall; Sl = slope; LD = lineament density; DD = drainage density; LU = land use; DR = distance to river; WT = water table depth.

Around the world, different methods have been used in delineating GWPZs such as integration of remote sensing and GIS with resistivity data [77], influence factor (IF) [47,51,66], statistical methods [78,79], groundwater modeling [80], and analytical hierarchy process (AHP) [63,74,81]. These methods have been proven as reliable and effective, and have been used by many researchers. Among those, AHP is advisable in cases of segregating multiple substitutes to a set of pairwise comparisons followed by the incorporation of the

result. Propounded by [82,83], AHP is also recommended when there is a lack of sufficient valid data for analysis [84–86]. AHP approach has been broadly applied in many fields of natural resources management, regional planning, and environmental impact assessment e.g., [56,87]. In the present study, AHP is integrated with RS-GIS techniques for the identification of GWPZs in the Shatt Al-Arab basin. Similar to [72,76,88–90], weights are allocated to the different parameters and their feature classes based on extensive literature reviews and expert knowledge using the AHP method. The integration of RS-GIS with AHP results in the conversion of data to obtain valuable information for managers and policymakers [91]. Therefore, the objective of this study is to define the GWPZs of the Shatt Al-Arab basin through the integration of RS-GIS with AHP. For this purpose, we utilized nine thematic layers (i.e., lithology, rainfall, geomorphology units, slope, drainage density, soil features, land use/land cover, distance to river, and lineament density) in the analysis. This study will be a useful tool for groundwater resources planners and managers when constructing sustainable groundwater plans in this region.

2. Study Area

The areas that drain to the Shatt Al-Arab River encompass the Tigris and Euphrates basins in addition to the Karun and Karkheh sub-basins (Figure 1). The Shatt Al-Arab River, developed by the confluence of the Tigris and Euphrates rivers at the city of Qurnah, flows to the southeast for around 100 km before it forms the borderline between Iran and Iraq for the last 90 km of its waterway until emptying into the Arabian Gulf. The total area discharging to the Shatt Al-Arab is around 143,111 km^2, excluding the Tigris and Euphrates basins (upstream of Qurnah), but including the Karun and Karkheh sub-basins. The Karun River stems from the Zagros Mountains in Iran, flows to the west through valleys and ridges to the city of Ahvaz, and continues towards the Shatt Al-Arab [92]. The Karkheh River also originates from the Zagros Mountains in Iran and flows to the south, and then turning northwest and is absorbed by the Hawizeh Marsh that straddles the Iran–Iraq border and eventually flows into the Shatt Al-Arab through the Swaib River (around 15 km south of Qurnah). The Shatt Al-Arab basin, a trans-boundary basin shared by Iraq and Iran, is situated in both Mesopotamia zone and Zagros structural zone. The Mesopotamia Zone, which is essentially covered by Quaternary sediments, consists mainly of three subzones; Tigris, Euphrates, and Zubair subzone [93]. The Tigris and Euphrates subzones are situated outside the Shatt Al-Arab basin whereas the Zubair subzone is situated within the basin. The Zubair subzone is characterized primarily by clastic lithology, while limestone is restrained to its upper parts [94]. The Zubair subzone is distinguished by many elongated folds that take N-S to NW-SE directions outlining the major oil fields in Basra Governorate [95]. These folds, of the Late Cretaceous age, are anticline folds with an appearance to basement rocks that are influenced by faulting [96]. On the other hand, the Zagros structural zone is characterized by thick sedimentary sequences that range in age from Cambrian to recent. The geological investigations indicate that the area was subjected to rifting movements during the Permian-Triassic and collision during the Tertiary [97]. Structurally, the Zagros Mountains consist of a series of ranges constituted from hundreds of anticlines and synclines arranged "en-echelon". The cores of the anticlines in the western part consist primarily of Cretaceous limestone and dolomite, while in the center they consist essentially of Eocene limestone. In the marginal western parts, many of the anticlines expose the Oligo-Miocene limestone and the Miocene gypsiferous marl [98]. The climate in the Iraqi part of the basin is mainly hot and arid with average temperatures varying from 9 °C in winter to 42 °C in summer, and an annual precipitation range of 100–175 mm [99]. In contrast, the Iranian part of the basin is characterized by cold winters and mild summers. Average temperatures vary from −25 °C in winter to 37 °C in summer, and annual precipitation ranges from 100 to 500 mm [99]. The basin's population is estimated at 11 million with an annual population growth rate of 2.6%. The average annual discharge is around 74 billion cubic meter (BCM) of the Shatt Al-Arab River into the Arabian Gulf. The total annual discharge is measured as follows: the Karkheh River

contributes of 5.8 BCM; the Karun River of 24.5 BCM; the Tigris River of 25.7 BCM (measured at the city of Kut); and the Euphrates River of 17.6 BCM (measured at the city of Hindeyah) [92].

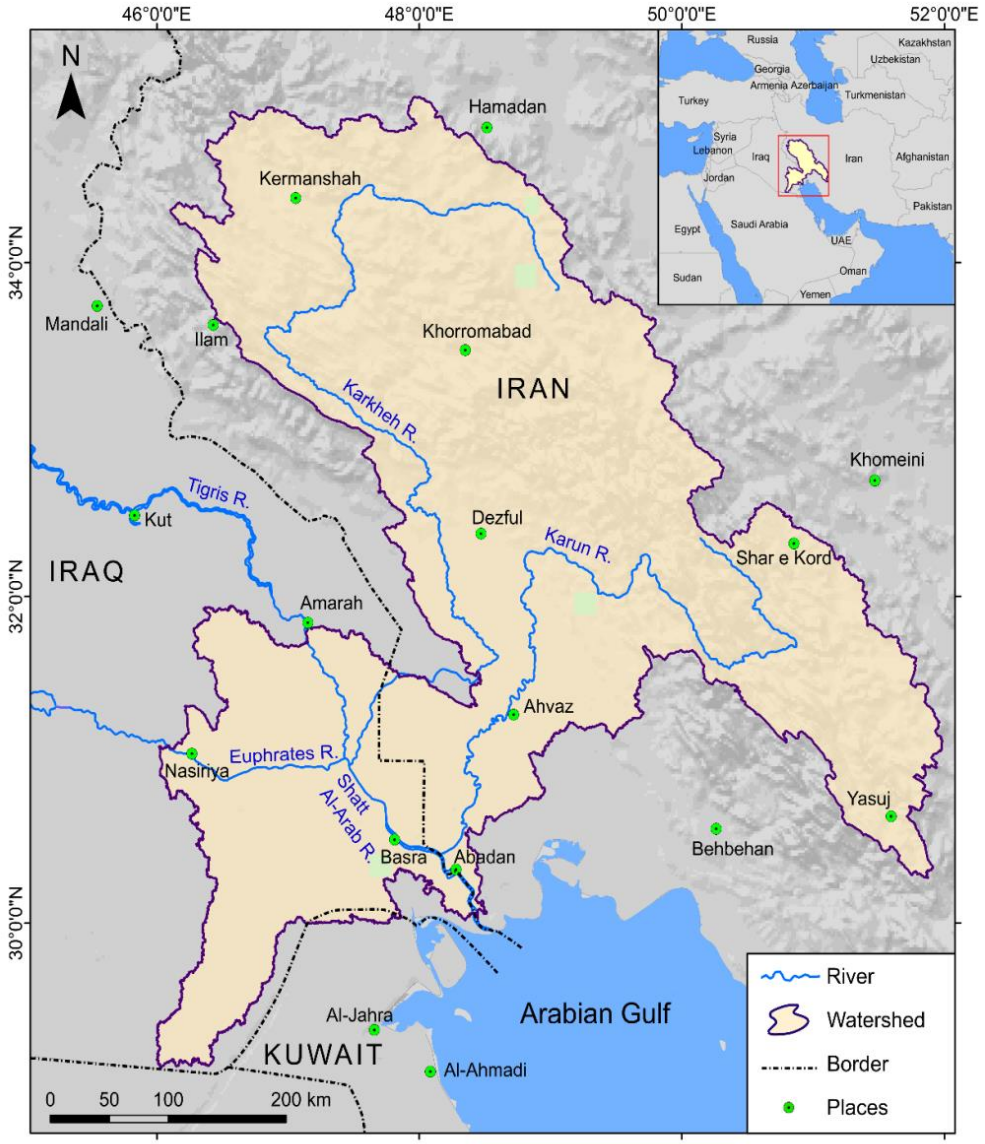

Figure 1. Site map of the trans-boundary Shatt Al-Arab basin (Iraq-Iran) with the Shatt Al-Arab River and its major tributaries.

3. Methods

3.1. Analytic Hierarchy Process (AHP)

The current study depends on the compilation of RS and GIS databases for preparing the GWPZs map. Nine controlling parameters were used for delineating the GWPZs (namely, slope, drainage density, rainfall, lithology, soil features, geomorphology units, land use/land cover, lineament density, and distance to river). The thematic maps of these parameters were tested by the AHP method using normalized weights to evaluate the GWPZs of the basin. The application of AHP needs scientific experience along with solid evidence [100] as well as an assessment of matrix consistency [54,84]. Similar to [101], we implemented the AHP technique by (i) selection of parameters controlling groundwater recharge, (ii) performing a pairwise comparison matrix, and (iii) assigning relative weights, and evaluating the matrix consistency (Figure 2).

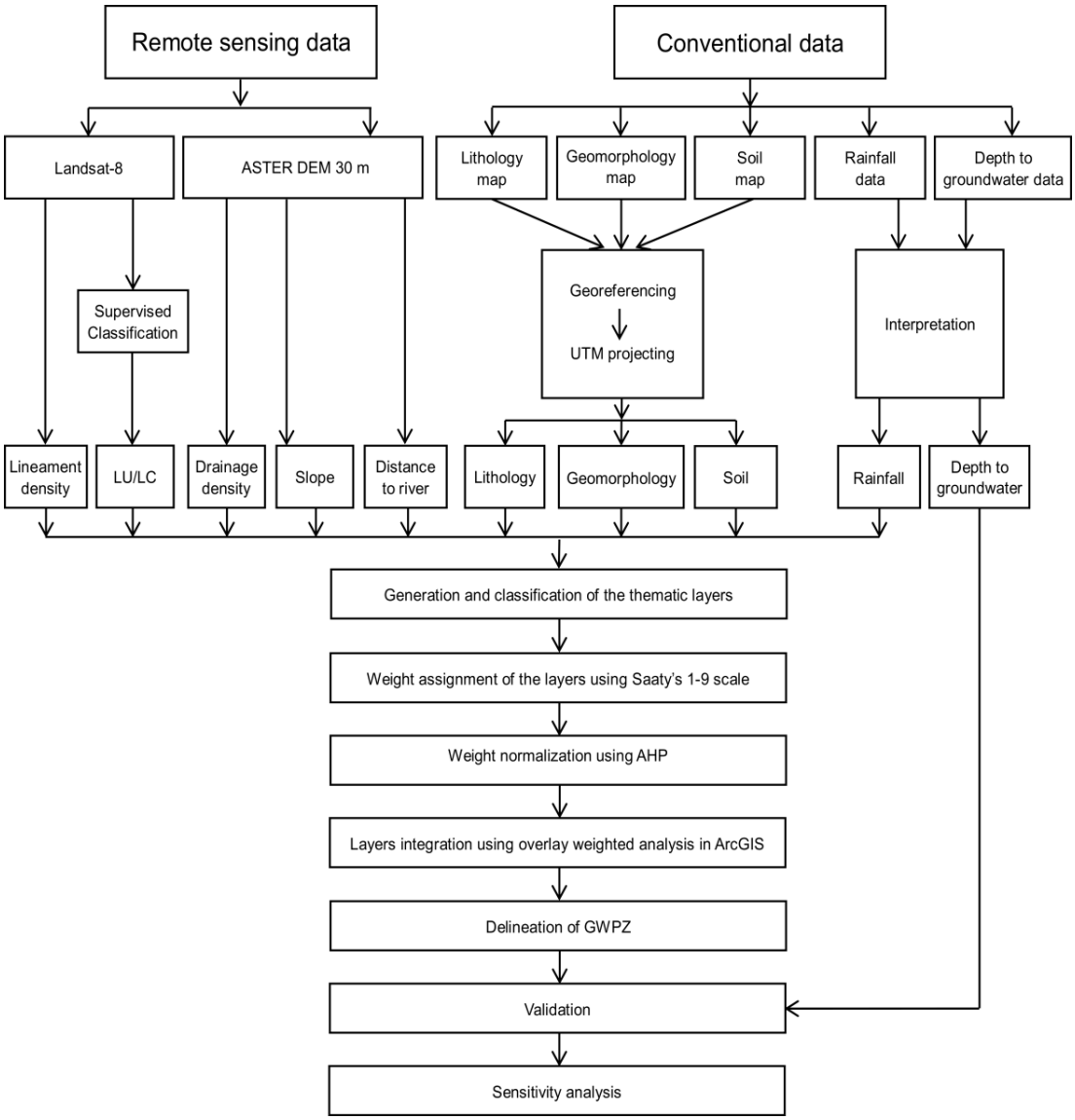

Figure 2. Flowchart for the identification of groundwater potential zones (GWPZs).

3.1.1. Selection of Parameters Controlling Groundwater Recharge

The evolution and flow of groundwater are mainly controlled by material features of the lithology, near-surface and sub-surface soil features, structure, and drainage patterns, whereas replenishment is influenced by rainfall, land use type, and infiltration rates [102]. Groundwater potentiality mapping can be achieved by investigating the controlling factors on groundwater movement, storage, and occurrence [75,103]. In the current study, nine thematic layers (i.e., slope, drainage density, land use/land cover (LULC), rainfall, soil features, lithology, geomorphologic units, lineaments, and distance to river) have been established and integrated for producing a groundwater potential zones map. These nine layers were explored and digitally mapped as thematic layers using the GIS environment with the aid of ArcGIS 10.4.1. The factors were used to represent: rainfall as the major source of water; slope, which drives the water flow energy; drainage density, which controls the runoff distribution and infiltration rates; lithology, which controls infiltration, movement, and storage of water; geomorphology units, which determine surface runoff and infiltration; soil features, which govern the infiltration rates; distance to river, which de-

termines the effective infiltration zones; land use/land cover, which affects the recharge processes; and lineaments, which increase hydraulic conductivity [54].

3.1.2. Pairwise Comparison Matrix

We created a pairwise comparison matrix according to the number of thematic layers for the GWPZs mapping [82,83]. Each input of the comparison matrix describes the effect of the row layer in relation to the column layer. The importance of a layer on groundwater potentiality related to another layer was graded based on the Saaty's 1–9 scale, where 1 expresses an equal impact of the two layers, and 9 represents the utmost impact of a row layer compared with a column layer [82,83] (Table 3). In other words, the low weights suggest low groundwater potentials, while the high weights imply high groundwater potentiality [104]. Similar to [72,76,88–90], we assigned the significance of the thematic layers (and later the rank to their feature classes) based on extensive literature reviews (e.g., Table 2) and experts knowledge as explained below.

Table 3. The one-to-nine scale of parameters significance [82].

Strength of Significance	Explanation
1	Equal significance
3	Medium significance
5	Strong
7	Very strong significance
9	Maximum significance
2, 4, 6, and 8	Interim number between two adjacent numbers

The reviews of both related literature and expert opinions indicated that different parameters impose a different impact on groundwater potentiality. For example, these reviews showed that lithology plays the main role in the evolution and flow of groundwater, and therefore was selected as the first layer and placed in the first row and first column of the comparison matrix in the current study (Table 4). Similarly and based on such reviews, we selected rainfall as the second most significant parameter since it represents the main source of water recharge [65]. Geomorphological units with corresponding features were selected as the third most important parameter since geomorphology represents an important criterion for demarcating groundwater potential zones [68,105]. Slope highly controls the infiltration of rainfall to the ground [106], and was selected as the fourth factor in the hierarchy. Drainage density, which has a negative correlation with permeability and consequently infiltration rate [107,108], was selected as a fifth parameter. Distance to river is an important factor, especially in arid regions because the occurrence of alluvial layers is generally situated near rivers [73], and was considered to be the sixth factor. The soil grain size was selected as the seventh factor in the hierarchy because infiltration and permeability are directly dependent on soil grain size and related pore size features [67,109]. Land use and lineament density have the least impact on groundwater recharge and thus were allocated the lowest importance. To define the priority and rank of the parameters, we created a pairwise comparison matrix based on the AHP method (Table 4). Priorities were assigned according to the one-to-nine point scale to each pair of layers. For example, lithology has more importance than rainfall for groundwater potentiality and was thus given a value of 2 (Table 4). The eigenvector expresses the ordering of layer influence on groundwater potentiality [110]. The normalized principal eigenvector in the current study was calculated using the excel sheet created by [111] (Table 4).

Table 4. A (9 × 9) pairwise comparison matrix for the analytic hierarchy process (AHP)-based groundwater potential (GWP) zoning.

	Lt	Rf	Ge	Sl	DD	DR	So	LULC	LD	Normalized Principal Eigenvector
Lt	1	2	3	3	3	2	2	4	4	24.06%
Rf	1/2	1	1	1	2	2	3	3	3 1/3	15.05%
Ge	1/3	1	1	1 3/7	1 3/7	2	3	3	3 1/3	14.52%
Sl	1/3	1	2/3	1	4/5	2	4/5	2	2	9.96%
DD	1/3	1/2	2/3	1 1/4	1	2	1/2	2	2	9.38%
DR	1/2	1/2	1/2	1/2	1/2	1	3	1 3/7	2	9.02%
So	1/2	1/3	1/3	1 1/4	2	1/3	1	1 1/9	1 1/4	7.94%
LULC	1/4	1/3	1/3	1/2	1/2	2/3	8/9	1	2	5.60%
LD	1/4	2/7	2/7	1/2	1/2	1/2	4/5	1/2	1	4.47%
Sum	4.0	7.0	7.9	10.4	11.7	12.5	15.0	18.0	20.9	
Total										100.00%

Lt = lithology; Rf = rainfall; Ge = geomorphology; Sl = slope; DD = drainage density; DR = distance to river; So = soil; LULC = land use land cover; LD = lineament density.

3.1.3. Assessing Matrix Consistency

The principal eigenvalue (λ_{max}) represents a function for the matrix divergence from consistency [85]. In other words, a pairwise matrix is considered consistent only when λ_{max} is equal or more than to the number of the layers examined (9 layers in the present study); otherwise, a new matrix must be constructed [82,83]. The principal eigenvalue (λ_{max}) of Table 5 was achieved by the addition of products of parameter columns sum in the pairwise matrix in Table 4 and eigenvectors in Table 4. A principal eigenvalue of 9.558 for a 9*9 matrix was obtained and used for the computation of the consistency index (Table 5). The normalized weights were verified for consistency by computing the consistency ratio [112]. The allocated weights are considered consistent only if the consistency ratio is equal or less than 10%; or else, these weights must be re-assessed to minimize inconsistency [113]. According to [83], the computation of the consistency ratio involves calculating the consistency index (CI):

$$CI = \frac{\lambda_{max} - n}{n - 1} \quad (1)$$

where λ_{max} denotes the principal eigenvalue, and n represents the number of parameters. Thus, the CI in this study is:

$$CI = (9.558 - 9)/9 - 1 = 0.0699 \quad (2)$$

Table 5. Computation of the principal eigenvalue (λ_{max}).

	Column Sums (Row 11 of Table 4)	Eigenvectors (Column 11 of Table 4)	Parameter Rank
	(1)	(2)	(1) × (2)
Lt	4.0	0.24	0.96
Rf	7.0	0.15	1.05
Ge	7.9	0.15	1.14
Sl	10.4	0.10	1.04
DD	11.7	0.09	1.10
DR	12.5	0.09	1.13
So	15.0	0.08	1.19
LULC	18.0	0.06	1.01
LD	20.9	0.04	0.93
Sum (λ_{max})			9.558

Lt = lithology; Rf = rainfall; Ge = geomorphology; Sl = slope; DD = drainage density; DR = distance to river; So = soil; LULC = land use land cover; LD = lineament density.

The consistency ratio (CR) was then computed according to:

$$CR = \frac{CI}{RI}, \quad (3)$$

where RI represents the random index which is given in Table 6 for different n values. In the current study, RI equals 1.45 for nine parameters. Therefore, CR is:

$$CR = 0.0699/1.45 = 0.048 = 4.8\% \quad (4)$$

where CR of 4.8% (less than 10%) is admissible to conduct the weighted overlay analysis to integrate the weighted parameters for the GWPZs mapping.

Table 6. Ratio index (RI) for various n scores [82,83].

N	3	4	5	6	7	8	9	10
RI	0.58	0.89	1.12	1.24	1.32	1.41	1.45	1.49

3.2. Identification of Groundwater Potential Zones

Groundwater potential index (GWPI) is a unitless value that expresses the GWPZs in a particular area that can be calculated according to [114]:

$$GWPI = \sum_{w=1}^{m} \sum_{j=1}^{n} (W_j \times X_i) \quad (5)$$

where W_j represents the normalized weight of the j parameter, X_i refers to the weight of the i class of the parameter, m denotes the number of the parameters, and n denotes the number of classes within a specific parameter. For each grid, the GWPI was computed according to the equation:

$$\begin{aligned} GWPI = {} & Lt_w Lt_r + Rf_w Rf_r + Ge_w Ge_r + Sl_w Sl_r + DD_w DD_r + \\ & DR_w DR_r + So_w So_r + LULC_w LULC_r + LD_w LD_r \end{aligned} \quad (6)$$

where Lt, lithology; Rf, rainfall; Ge, geomorphology; Sl, slope; DD, drainage density; DR, distance to river; So, soil; LULC, land use/land cover; and LD, lineament density. The symbol 'w' expresses the weight of a thematic layer (column 4 in Table 7), and the symbol 'r' expresses the rating of subclasses (the rank) in each layer (column 5 in Table 7).

Table 7. Classification of parameters controlling the GWPZs in the Shatt Al-Arab basin.

Factor (Unit)	Class	Groundwater Potentiality	Parameter Weight	Class Rank
Lithology	Evaporites	Very low	24	1
	Metamorphic	Low		4.5
	Plutonic Igneous	Low		8
	Volcanic Igneous	Low		11.5
	Siliciclastic Sedimentary	Medium		15
	Mixed Sedimentary	High		18.5
	Carbonate Sedimentary	High		22
	Unconsolidated Sediments	Very high		24
Rainfall (mm/yr)	<100–200	Low	15	1
	200–300	Moderate		5
	300–400	High		10
	400–500	Very high		15

Table 7. *Cont.*

Factor (Unit)	Class	Groundwater Potentiality	Parameter Weight	Class Rank
Geomorphology unit	Floodplain	Very high	14	14
	Bajada	Very high		14
	Valley fill	Very high		14
	Pediplain	High		9
	Pediment	Moderate		4
	Badland	Very low		1
	Cuesta	Very low		1
	Denudational hill	Very low		1
Slop (degree)	<10	Very high	10	10
	10–20	High		7
	20–30	Moderate		5
	30–40	Low		3
	>40	Very low		1
Drainage density (km/km^2)	<0.75	Very high	9	9
	0.75–1.5	High		7
	1.5–2.25	Moderate		5
	2.25–3	Low		3
	>3	Very low		1
Distance to river (km)	0–35	Very high	9	9
	35–70	High		7
	70–105	Moderate		5
	105–140	Low		3
	>140	Very low		1
Soil	Clay	Extremely low	8	1
	Silty clay	Very low		2
	Sandy clay	Low		3
	Clay loam	Moderate		4
	Loam	High		5
	Loamy sand	Very High		7
	Sand	Extremely high		8
Land use/land cover	Urban	Very low	6	1
	Shrub land (36%)	Low		3
	Cropland (12%)	Moderate		4
	Bare land (~50%)	High		5
	Water	Very high		6
Lineament density (km/km^2)	<0.018	Very low	4	1
	0.018–0.071	Low		1.75
	0.071–0.143	Moderate		2.50
	0.143–0.232	High		3.25
	0.232–0.391	Very High		4

3.3. Digital Elevation Model and Watershed Delineation

The digital elevation model (DEM) data were obtained from EARTHDATA Search (https://search.earthdata.nasa.gov/search) by outlining the study area and selecting the Advanced Spaceborne Thermal Emission and Reflection Radiometer (ASTER) Global Digital Elevation Model V003. We downloaded the images from (ASTER) DEM data of 30 m resolution. These images were then added to ArcGIS 10.4.1 and merged (mosaic) using "Data Management Tools > Raster > Raster Dataset > Mosaic to New Raster. Next, we identified the Universal Transverse Mercator (UTM) zone and re-projected the merged map. The projected DEM was corrected using Spatial Analyst Tool > Hydrology > Fill tools. The tool "Hydrology" was utilized to determine the flow direction and flow accumulation. We then generated the drainage lines using the "Map Algebra" tool. An outlet to the watershed was allocated by using the Catalog window and creating a shapefile.

Next, we used the "Watershed" tool, a tool within the "Hydrology" tool, to create the Shatt Al-Arab watershed boundary by inputting the flow direction file and outlet file in the tool "Watershed" window.

3.4. Factors Influencing Groundwater Recharge Zones

3.4.1. Lithology

Lithology has a principal impact on the occurrence and movement of groundwater as it highly controls the infiltration and flow processes [103]. Ref. [115] stated that the rock type can substantially influence the groundwater recharge potential. Similarly, Ref. [116] found that lithology affects the recharge by governing the water percolation. Some investigations have neglected the lithology parameter in GWP zoning by considering the drainage features and lineament density as a measure of primary and secondary porosity; however, we followed [60] by including the lithology in our analysis to minimize the uncertainty in estimating drainage and lineament densities. The 1/3,750,000 lithological map of the basin was achieved by the University of Hamburg website (https://www.dropbox.com/s/9vuowtebp9f1iud/LiMW_GIS%202015.gdb.zip?dl=0) to describe the lithology in the study area [117]. The map was then added to ArcGIS, and the study area was extracted using the tools Analysis Tools > Extract > Clip. Lithological categories classification was done according to the classes available in the lithology classification website (https://www.clisap.de/fileadmin/B-Research/IA/IA5/LITHOMAP/).

3.4.2. Rainfall

Groundwater recharge is controlled by various factors with rainfall playing a key role since it represents the main source of groundwater recharge [65,118]. The annual mean rainfall for the period from 2011 to 2018 in the study area was obtained from the Climate Research Unit (www.cru.uea.ac.uk/data). We then selected "Main webpage for the high resolution gridded datasets" to download rainfall data. The rainfall data were converted to a raster layer using the tools Multidimensional Tools > Make NetCDF Raster Layer. We then converted the raster layer to points using the tools Conversion Tools > From Raster > Raster to point. These points were interpolated through the tools Spatial Analyst Tools > Interpolation > Kriging to obtain a rainfall contour map. The rainfall map for the study area was extracted using the tools Spatial Analyst Tools > Extraction > Extract by Mask.

3.4.3. Geomorphology

Geomorphological units, physical features of the earth's surface and the near-surface underground, represent significant aspects in hydrogeological investigations, evaluation of topography, and delineation of groundwater resources [119]. Previous studies e.g., [64,68,70,76,105,120] have incorporated geomorphology features as a significant parameter for demarcating GWPZ. The geomorphic features in the current study were georeferenced and digitized from images.

3.4.4. Slope

Slope depicts the local and regional relief which has a significant influence on groundwater recharge into the aquifers [121]. The slope gradient directly controls the surface water infiltration [122] and is widely used in the delineation of GWPZs [51]. A region of a high slope gradient has relatively low GWP due to the higher runoff. On the other hand, a low slope gradient constrains the water flow and hence stimulates the infiltration rate [70]. After generating the DEM and drainage lines and creating the watershed boundary in Section 3.3, we generated the slope using the tools Spatial Analyst Tools > Surface > Slope in ArcGIS 10.4.1.

3.4.5. Drainage Density

Drainage density is the cumulative length of the stream segments of all orders in a region divided by the region area [123]. Drainage patterns are derived from surface and

sub-surface features such as texture, fracture, underlying lithology, and hydrogeological features [124]. Drainage density represents a good indicator to predict the infiltration rates and feature the relation between surface runoff and permeability in a terrain [70]. Terrains of high drainage densities have relatively low recharge rates, whereas areas of low drainage densities have higher recharge rates [125]. High drainage densities are favorable for runoff and thus result in a poor GWPZ and vice versa [62]. Drainage density in the current study was calculated using the tools Spatial Analyst Tools > Density > Line Density in ArcGIS 10.4.1.

3.4.6. Distance to River

Distance to hydrographic networks is important in hydrogeological studies because it is noted that the presence of local alluvial layers is located essentially near the river courses especially in semi-arid regions [73]. Areas close to rivers are favorable for effective infiltration and consequently groundwater recharge. In contrast, it is difficult to find alluvial layers in areas beyond a distance of 600 m [126]. Distance to river was determined by selecting Spatial Analyst Tools > Map Algebra > Raster Calculator. In the Raster Calculator window, we entered the following command:

$$\mathrm{Con}(\text{"FlowACC.tif"} > 4000000, 1)$$

where Con represents condition, FlowACC.tif represents the flow accumulation that was prepared in Section 3.3, and 4,000,000 is a value that enabled us to create the major river courses in the study area (i.e., Tigris, Euphrates, Karun, and Karkheh rivers). The resulting raster file was then converted to lines using the tools Conversion Tools > From Raster > Raster To Polyline. To classify the distance to major rivers, we used Spatial Analyst Tools > Distance > Euclidean Distance.

3.4.7. Soil Features

Soil has a significant control on the infiltration and percolation rates into an aquifer [127]. Soil grain size, shape, and arrangement and the corresponding pore system can highly affect the vertical and lateral water movement [109]. The soil map was obtained from Geo Network Web Portal for Food and Agriculture Organization (FAO) Soil Map (http://www.fao.org/geonetwork/srv/en/metadata.show%3Fid=14116). From FAO website, we downloaded data from "Digital Soil Map of the World—ESRI Shapefile format". Furthermore, soil categories were obtained from SWAT Soil Data (http://www.indiaremotesensing.com/p/s.html). The soil map was added to ArcGIS 10.4.1 and geo-referenced to the UTM projected coordinate system. We extracted the study area using the tools Analysis Tools > Extract > Clip. The map was then geo-coded to each soil type at different categorical levels in soil classification according to the classes obtained from the SWAT Soil Data.

3.4.8. Land Use/Land Cover (LULC)

LULC is reported to have an impact on the existence and development of groundwater in an area [128]. Built-up lands are typically accompanied by a reduction in the infiltration rate due to a lack of permeable surfaces. In contrast, forests and agricultural lands allow more infiltration of water since the vegetative cover can retain water and facilitate infiltration [129]. Ref. [30] discovered that water bodies have the highest infiltration rate followed by forests, cropland, settlements, and industrial/quarry respectively. Data on catchment LULC were extracted from land cover databases on the Earth Explorer (https://earthexplorer.usgs.gov/). We outlined the study area and selected dataset > Landsat > Landsat collection 1 Level-1 > Landsat 8 OLI/TIRS C1 Level-1. From "Additional Criteria", we chose Land Cloud Cover and Scene Cloud Cover less than 10% to obtain images with minimum cloud cover. Images were then added to Erdas and processed. For image enhancement in Erdas, we selected Raster > Spatial > Convolution, added the images, and selected 3 × 3 Edge Enhance. To remove black pixels, we selected Manage Data > Pyramids and Statistics > Compute Pyramids and Statistics > and ticked Set NoData

Value. Then we selected Pyramids and Statistics > Compute Pyramids and Statistics > and ticked each of Clear NoData Value, Compute Statistics, and Compute Pyramid Layers. LULC was classified using the supervised classification in ERDAS IMAGINE 2014. In the supervised classification, we selected and digitized polygons and placed these polygons in an "Area of Interest" layer to create the signature files. In other words, we drew several polygons around a specific land use type and then created a related signature to make this land use type a certain class. The same procedure was done for the other land use types creating multiple classes representing the various land use types in the study region. The supervised classification method is a more time-consuming method, but the benefits include higher overall accuracy compared with the unsupervised method [130].

3.4.9. Lineament Density

A lineament is a linear property that expresses the underlying structural features such as fractures, faults, cleavages, and discontinuity surfaces. Lineaments represent the simple and complex linear features of structures, with parts that are arranged in a rectangular or moderately curved mode, and which differ from the arrangement of the adjacent features and reflect some subsurface feature [131]. Lineaments are often used in mineral exploration studies [132], geothermal resources [133], soil erosion studies [134], earthquakes [135], and the identification of GWPZs [51,94]. Regions with high lineament densities indicate high permeable zones and hence represent good GWPZs [103]. Lineament density (L_d), which is the length of lineament segments in a particular region per its area, is calculated according to the following equation:

$$L_d = \frac{\sum_{i=1}^{i=n} L_i}{A} \quad (7)$$

where $\sum_{i=1}^{i=n} L_i$ represents the length of lineament lines, and A represents the area. Elevated lineament densities indicate good secondary porosity and accordingly suggest good recharge zones. The lineament density is generally divided into very high, high, moderate, low, and very low [136]. A lineaments map of the Shatt Al-Arab basin was created using the Landsat-8 (Thematic Mapper and Operational Land Imager) satellite image and extracted using PCI Geomatica Software [137]. In PCI Geomatica, the image was added and enhanced using "Enhancements" tool. Then, we selected Tools > Algorithm Librarian > Line: Lineament Extraction. The obtained map was then added to ArcGIS, and the lineament density was estimated by choosing the tools Spatial Analyst Tools > Density > Line Density.

3.5. Results Validation

The prospective zones of groundwater delineated by RS-GIS techniques are typically verified by comparison with existing borewells data. In the current study, however, such data are not available. Alternatively, depth to groundwater data were extracted from the peer-reviewed literature [138–143] for 99 wells distributed throughout the basin. We performed a comparative analysis between the depth to groundwater and the potential zones. The map of wells was projected on the GWPZs map to verify the effectiveness of the RS-GIS and AHP-based method in demarcating GWPZs in the study area.

3.6. Sensitivity Analysis

Sensitivity analysis offers significant facts on the impact of each influencing factor on GWPZs analysis [144]. Sensitivity analysis is an effective way to interpret groundwater potential index [145]. The layer-removal technique represents the groundwater potential sensitivity associated with eliminating one layer at a time [67,146] according to the following equation:

$$S = \left(\frac{\left| \frac{V}{N} - \frac{V'}{n} \right|}{V} \right) \times 100 \quad (8)$$

where V is the unperturbed, V′ is the unperturbed GWPI (i.e., GWPI when excluding one factor), and N and n are the numbers of factors used to compute V and V′, respectively. Next, in order to investigate the variation magnitude in groundwater potential zone types (i.e., very good, good, moderate, poor, very poor) caused by the removal of one layer at a time, the variation index [134] was calculated according to:

$$S_x^y = \left(\frac{A_{-x}^y - A_n^y}{A_n^y} \right) \times 100 \quad (9)$$

where x is the factor number, y is the zone type (i.e., very good, good, moderate, poor, very poor), S_x^y refers to the percentage variation in yth type of groundwater potential zone area owing to the removal of xth factor, A_{-x}^y is the yth type of groundwater potential zone area resulting from the removal of the xth criterion, and A_n^y is the yth type of groundwater potential zone area using all factors.

4. Results

The study area varies in elevation with the eastern regions having the highest elevation (1500–4400 m above sea level), whereas the western parts are much flatter with the lowest elevation (0–100 m) (Figure S1).

4.1. Factors Influencing Groundwater Recharge Zones

4.1.1. Lithology

The lithology thematic map distinguished eight lithological unites, viz; unconsolidated sediments, evaporites, metamorphic, plutonic igneous, volcanic igneous, siliciclastic sedimentary, mixed sedimentary, and carbonate sedimentary rocks (Figure S2). The southwestern areas of the basin consist mainly of unconsolidated sediments (account for 42% of the total basin area). On the other hand, the eastern areas consist significantly of carbonate sedimentary rocks and mixed sedimentary rocks that comprise around 44% of the total basin area. The western parts of these areas are composed primarily of Cretaceous limestone and dolomite, while the center consists essentially of Eocene limestone [98]. The extreme northeastern parts are composed of metamorphic, siliciclastic sedimentary, and igneous rocks that in total form around 13% of the basin area.

4.1.2. Rainfall

The overall feature of the mean annual rainfall is that it has the highest levels on the northern parts, and exhibits a southwards gradient towards the Gulf. The four rainfall zones defined in this study are 400 to 500, 300 to 400, 200 to 300, and 200 to less 100 mm yr^{-1} (Figure S3).

4.1.3. Geomorphology Units

We were able to distinguish eight geomorphological features according to their origin. These features are of denudational origins such as pediplain, badland topography, and denudational hills; of depositional origin such as floodplain, pediments, valley fills, and bajada; and of structural origin such as cuesta (Figure S4). Floodplains in the current study stretch along the main course of the Shatt Al-Arab River. Bajada exists along the foothills in the middle parts of the basin. Valley fills prevail in the northwestern parts of the study area. While pediplain occupies large areas of the southern parts of the basin, pediments extend at the margins of the pediplain. Badland and cuesta mainly appear in the northern parts of the basin. Denudational hills spread along the eastern margins of the study area (Figure S4).

4.1.4. Slope

Five slope classes were detected in the present study (i.e., <10°, 10–20°, 20–30°, 30–40°, and >40°). A substantial area of the basin falls within the first slope category (i.e., <10°).

This category, situated in the southwestern parts, has the gentlest slope and lowest topographic elevation. Other slope classes exist mainly in the eastern parts of the basin (Figure S5).

4.1.5. Drainage Density

The drainage density of the Shatt Al-Arab basin is categorized into five classes (i.e., <0.75 km/km^2 which covers 17% of the basin area; 0.75–1.5 km/km^2 covers 41%; 1.5–2.25 km/km^2 covers 33%; 2.25–3 km/km^2 covers 8%; and more than 3 km/km^2 covers 1%). Thus, most of the study area has low to moderate drainage densities (Figure S6).

4.1.6. Distance to River

The distance to rivers in the Shatt Al-Arab basin is categorized into five classes. The first class (i.e., 0–35 km) covers more than 50% of the basin area. On the other hand, the other four classes (i.e., 35–70, 70–105, 105–140, and >140 km) represent less than 50% of the study area (Figure S7).

4.1.7. Soil Features

The soil map of the study area is classified into seven soil categories, viz., loam, clay loam, loamy sand, sand, clay, sandy clay, and silty clay (Figure S8). More than 90% of the soil types in the Shatt Al-Arab basin are of loam and clayey loam type. Loam soils occur in the northeastern parts, whereas clayey loam soils mostly prevail in the middle areas of the basin. Loamy sand and sand soils appear in the southern parts of the basin and represent around 6% of the total soil types. Clayey soils (i.e., sandy clay, silty clay, and clay) compose around 2% of the soil types.

4.1.8. Land Use/Land Cover

The bare land, shrub land, and cropland, are the main LULC types in the Shatt Al-Arab basin (Figure S9). On the other hand, urban and water/wetland land use represent only a small percentage of the LULC types prevailed in the Shatt Al-Arab basin.

4.1.9. Lineament Density

Lineament densities in the basin vary from <0.018 to 0.391 km/km^2 (Figure S10). High lineament density is generally situated at the northeastern parts of the basin taking a somewhat elongated form in the NW-SE direction. The general trend of the lineaments in the study area displays a rapid density decrease towards the southwest.

4.2. Groundwater Potential Zoning

The GWPZs map of the Shatt Al-Arab basin reveals five distinct classes (zones) (Figure 3). These zones that represent very good, good, moderate, poor, and very poor groundwater recharge potentiality in the basin cover 12,136, 66,578, 51,836, 11,608, and 953 km^2, respectively. Typically, the zones of high groundwater potentiality coincide with areas of a high groundwater table which is controlled by different factors. In the current study, the very good GWPZ is situated in the northwestern part, and the good GWPZ covers the southwestern parts of the basin. On the other hand, moderate, poor, and very poor GWPZs cover the eastern parts of the study area (Figure 3).

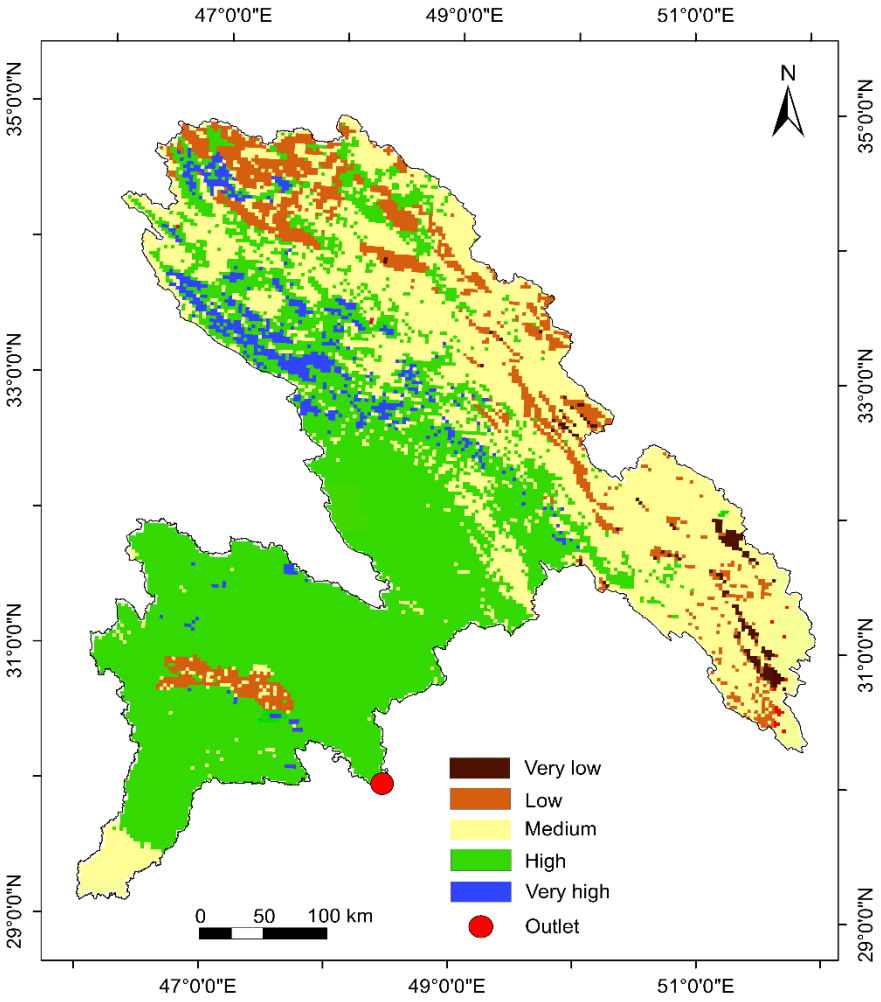

Figure 3. GWPZs of the study area.

4.3. Results Validation

The validation results showed that, out of 99 wells, 67 wells accurately match, 16 wells partially match, and 16 wells do not match with the groundwater potential map zonation (Table S1; Figure 4). For example, wells numbered 9, 10, and 12 that show very shallow, shallow, and medium depth to groundwater, respectively, are located in the very good, good, and moderate GWPZ, respectively (Table S1).

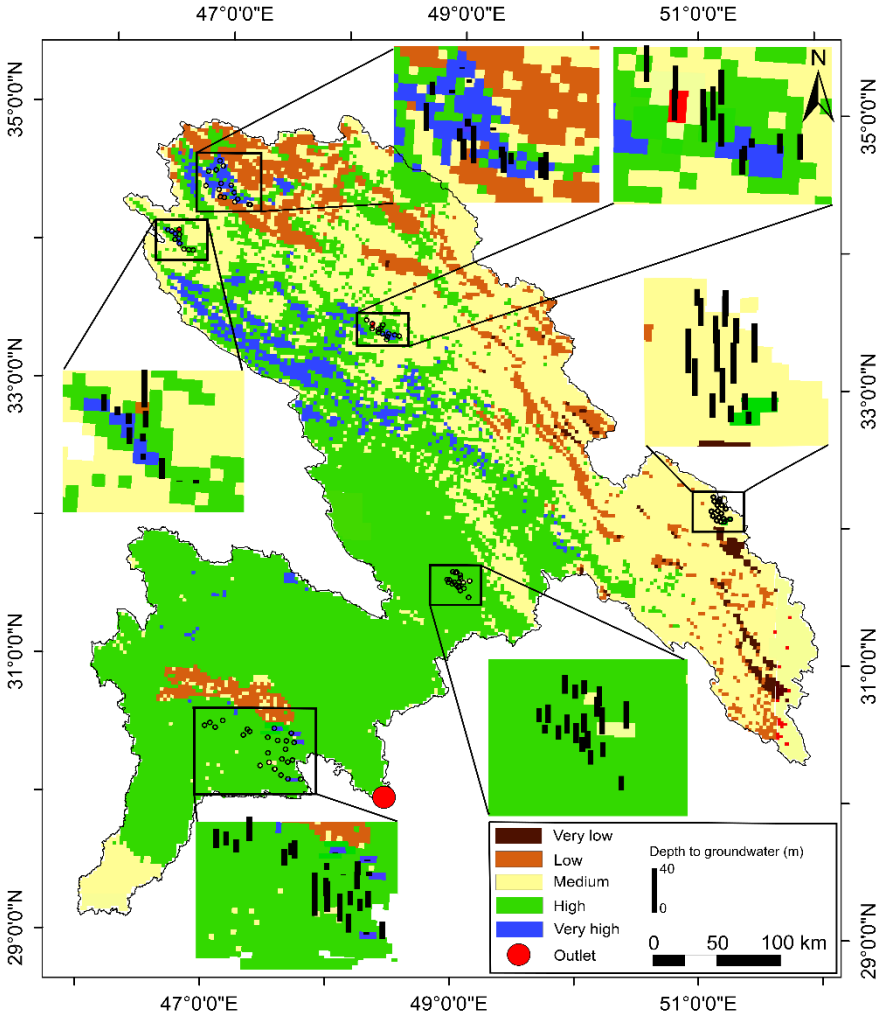

Figure 4. Projection of depth to groundwater of wells on the GWPZs map.

4.4. Sensitivity Analysis

According to the sensitivity analysis (Table 8), the lithology factor has the largest variation index (2.78%). Likewise, geomorphology features also influence the GWPZs assessment reasonably (variation index is 1.27%, Table 8). The elimination of the LULC also affects the variations of the GWPZs assessment (variation index of 1%). Similarly, the GWPZs seem to be sensitive to the removal of rainfall and lineaments (variation index of 0.96 and 0.89%, respectively). The omission of soil, distance to river, slope, and drainage density has also contributed to the sensitivity variations; their mean values are 0.73, 0.72, 0.62, and 0.46, respectively (Table 8). The exclusion of each factor from the assessment changes the percentage area of the very poor, poor, moderate, good, and very good GWPZ. Drainage density and slope are the vital influencing parameters in identifying the GWPZs because their removal considerably increases the "Very good" GWPZ area by 83.5 and 80.4%, respectively (Table 9). In the same way, exclusion of geomorphology increases the "Good" GWPZ area by 32.7%. Moreover, the "Moderate" and "Poor" GWPZs areas seem to be sensitive to the omission of lithology because their removal increases the areas of these two zones by 38.5% and 70.6%, respectively (Table 9). Finally, the "Very poor" GWPZ category is influenced by the removal of soil features, distance to river, drainage density, and rainfall by 69.9, 50.8, 39.9, and 38.9%, respectively.

Table 8. Map elimination sensitivity analysis (one factor is eliminated at a time).

Factor Eliminated	Variation Index (%)			
	Min	Max	Mean	SD
Lithology	0.60	5.56	2.78	0.80
Geomorphology units	0.35	4.60	1.27	0.95
LULC	0.51	11.10	1.00	0.76
Rainfall	0.53	11.11	0.96	0.82
Lineament density	0.82	1.39	0.89	0.25
Soil features	0.95	2.19	0.73	0.33
Distance to river	0.78	1.39	0.72	0.25
Slope	0.35	1.52	0.62	0.28
Drainage density	0.49	2.32	0.46	0.31

Table 9. Zone category change under the elimination of each factor.

Factor Eliminated	Zone Category Change ((+/−) %)				
	Very Poor	Poor	Moderate	Good	Very Good
Lithology	6.7	70.6	38.5	−74.3	−100.0
Rainfall	38.9	−29.0	−14.2	−17.3	54.3
Geomorphology units	−6.7	−30.3	−28.3	32.7	−93.0
Slope	7.3	1.4	−5.9	−0.8	80.4
Drainage density	39.9	−0.6	−9.2	1.2	83.5
Distance to river	50.8	6.6	−1.4	−2.8	26.5
Soil features	69.9	12.3	0.9	−6.0	27.0
LULC	−9.3	−5.9	−7.7	3.1	66.5
Lineament density	8.8	−11.0	−4.8	1.2	70.9

5. Discussion

5.1. Factors Influencing Groundwater Recharge Zones

5.1.1. Lithology

The southwestern areas of the basin that consist mainly of unconsolidated sediments are primarily represented by fluvial sediments of the Euphrates and Tigris rivers and their tributaries [147]. These sediments have high porosity and permeability and were classified into a high GWPZ in the current study (Table 7). Similarly, carbonate sedimentary rocks generally have good permeability [148] and were allocated a high rank in groundwater potentiality classification (Table 7). Siliciclastic sedimentary rocks have moderate porosity and permeability and were assigned a medium rank. On the other hand, metamorphic, igneous rocks, and evaporites are typically associated with low porosity and permeability [148] and are normally assigned low ranks in lithology sub-classification [66,149] (Table 7).

5.1.2. Rainfall

Ref. [150] found that their regression plots of groundwater recharge versus rainfall displayed strong linear positive relationships. Thus, the four rainfall zones defined in this study (i.e., 400 to 500, 300 to 400, 200 to 300, and 200 to less 100 mm yr^{-1}) were assigned a very high, high, moderate, and low rank respectively in layer classification for groundwater potentiality (Table 7).

5.1.3. Geomorphology Units

Floodplains that consist of weathered deposits [151] represent a powerful permeable sector promoting partial bank recharge and subsurface flow [152]. Floodplains generally exhibit good groundwater potentiality owing to the high infiltration rate of their weathered material deposits [71,153], and hence were assigned a high rank in the current study (Table 7). Bajada comprises of detrital materials of various lithologies and grain sizes with good groundwater potential [152]. Valley fills consist of loose alluvial deposits along the

river valley floor originating from encompassing highlands [61]. This unit allows for high infiltration and has good groundwater potentiality [125]. Pediplain that is produced by the intensified weathering under semi-arid circumstances represents the final phase of the cyclical erosion [154]. This unit has good groundwater prospects. Pediments are gently sloping surfaces formed between hills and plains and generally associated with moderate groundwater yield [125]. Badland and denudational hills are typically associated with poor infiltration capacities [155]. Cuesta is a ridge or hill with a low slope on one edge, and a high slope on the other, and normally is unsuitable for groundwater occurrence [76].

5.1.4. Slope

Previous studies indicated that groundwater potentiality increases with gentle slope and low topographic elevation areas owing to the longer residence time for water to percolate [156–159]. The first slope category (i.e., <10°) that has the gentlest slope and lowest topographic elevation was categorized within 'very high' groundwater potentiality owing to the nearly-flat topography that promotes high infiltration rates. The areas with a slope of 10–20° are classified within 'high' groundwater potentiality due to their gently undulant terrains and moderate runoff potential. The areas with a slope range of 20–30° are categorized within 'moderate' groundwater potentiality due to their limited infiltration rates and relatively high runoff. The areas with slopes of 30–40° and more than 40° are recognized as 'low' and 'very low' groundwater potentiality respectively owing to their steeper slope that results in a higher runoff potential (Figure S5).

5.1.5. Drainage Density

There is a negative relationship between drainage densities in a region and groundwater recharge because high drainage densities lead to low infiltration rates [62]. Most of the study area has low to moderate drainage densities, which represents a positive influence on groundwater potential (Table 7).

5.1.6. Distance to River

The distance to river is important in groundwater potential zoning because the presence of alluvial layers is mostly located near the river courses [73]. A negative relationship is reported between distance to river and water supply from river [160]. As such, the closer the areas to rivers, the higher weights were assigned in groundwater potential calculations (Table 7).

5.1.7. Soil Features

Based on the literature review (e.g., work presented in Table 2), we found that irrespective of land use, both the top and the subsoil texture or grain size composition can remarkably control groundwater recharge. The control of soil on recharge rate can be ascribed to the variations in hydraulic conductivity and infiltration rate of various soil types [161]. Soil pore volume, pore size distribution, and pore continuity can greatly influence the water movement [109]. Sandy soils have a high percentage of macro pores with faster water infiltration rates compared with loamy soils. Loamy soils which own high percentages of middle size pores have higher infiltration rates than clayey soils which have the highest percentage of fine size pores [109,162,163]. Particular weights are allocated to each soil category based on the soil type and the related infiltration rate. Large areas of the basin are covered by loam and clayey loam soils and were assigned a high to intermediate priority in groundwater potential analysis. Loamy sand and sand soils were allocated a very high to extremely high weight. Clayey soils (i.e., sandy clay, silty clay, and clay) were assigned a low to extremely low weight (Table 7).

5.1.8. Land Use/Land Cover

Bare land, which occupies around 50% of the basin area, has higher groundwater recharge rates compared with other types of land use such as cropland and shrub land [164].

Cropland was assigned a higher score compared with shrub land and settlement land use since irrigation enhances the water quantity applied to the fields, and hence promotes the groundwater recharge [165]. Ref. [128] concluded that the replacement of rangelands with crop lands alters the direction of water flow from lateralward (discharge) to downward (recharge). Conversely, urban land use has low infiltration rates and capacities due to the impervious surfaces dominating in such type of land use [166], and thus has a very low rank in GWPZs assessment (Table 7).

5.1.9. Lineament Density

The direction NW-SE of the high lineament densities in the current study coincides with the Arabian–Iranian tectonic plate boundary. Lineaments features (e.g., faults, fractures, cleavages) are usually more concentrated at the plate margins because boundaries between tectonic plates are made up of a system of faults [167]. Lineaments, weak zones in the landscape that facilitate the movement of groundwater, are an important theme for GWPZs mapping since they have considerable control over the movement of groundwater [168,169]. Fractures in rocks enhance their secondary porosity and permeability and thus increase the groundwater movement [76]. Areas with high lineament density in the present study denote permeable zones, so reveal good groundwater potential zones (Table 7).

5.2. Groundwater Potential Zoning

A closer analysis of the map indicates that the distribution is a considerable consequence of the lithological influence. The very good and good GWPZs mainly encompass lithological units of unconsolidated sediments, carbonate sedimentary rocks, and mixed sedimentary rocks. It indicates that the areas where such lithological units dominated are the most promising areas for groundwater storage (Figure S2 and Figure 3). Similarly, geomorphology units, which are widely documented to have a remarkable impact on groundwater recharge, displayed a reasonable control on groundwater potential distribution in the current study. Geomorphological units that have good groundwater recharge capacities (e.g., floodplain and pediplain) prevailing in the southwestern parts of the basin are most likely contributing to the high groundwater potential in such parts. Similarly, valley fills that occur in the northwestern part of the basin, which also have high groundwater recharge capacities, can explain the very good GWPZ in this part (Figure S4 and Figure 3). Low slope areas in the southwestern part of the study area can partially rationalize the identified good groundwater potential in this part (Figure S5 and Figure 3). Likewise, the closer distances to the rivers in the southwestern part can enhance the groundwater potentiality in this part. The impact of the close distances to the rivers in the northern parts can be observed in the northwestern part which has a very good groundwater potentiality. Our results, however, show that the close distances to the rivers in the rest of the northern parts have almost no effect on GWPZ, and this can be attributed to the offset by the other parameters (e.g., lithology, geomorphology units, slope, drainage density, and land use) that have low groundwater potential ratings in such parts (Figure S7 and Figure 3). Water and bare land use, have high groundwater recharge weights, are dominated in the southwestern parts, and are most likely contributing to the higher GWPZ in such parts in the current study (Figure S9 and Figure 3). The rainfall impact can be observed in the northwestern part which has a very high groundwater potentiality. The southern parts have high groundwater potentiality despite the low rainfall amounts that these parts receive, and this can be ascribed to the other parameters mentioned above that have classes with high GWP in these parts (Figure S3 and Figure 3).

5.3. Results Validation

The groundwater depths highly fluctuate from one site to another in the basin, expressing the different geological settings and the spatial variations in the groundwater recharge rate throughout the basin. The southwestern part of the basin around the unconsolidated

sediments, floodplain and pediplain, low slope, flat topography, and bare land use is favorable for groundwater recharge potentiality and, hence, the depth to groundwater is shallow. In contrast, zones (generally in the eastern parts of the basin) with unfavorable lithology, geomorphology units, slope, and topography have low groundwater prospects and thus a relatively deep groundwater depth. Most of the "very shallow" groundwater territories are concentrated in the northwestern parts of the basin (Figure 4). The best groundwater prospects in this part can be attributed to the suitable conditions for groundwater recharge potentiality (i.e., highest rainfall, sedimentary rocks, valley fills, high soil porosity condition, low drainage density, and close distance to river) (Figure 4).

5.4. Sensitivity Analysis

According to the sensitivity analysis (Table 8), the lithology factor has the largest variation index. Besides its relatively high theoretical weight (i.e., 24%), lithology has high values in sub-classes that occupy most of the basin area. In other words, unconsolidated sediments, carbonate sedimentary, mixed sedimentary, and siliciclastic sedimentary rocks which comprise more than 90% of the basin have high sub-class ratings (Table 7). The removal of geomorphology features also influence the GWPZs assessment and this can be explained by the fact that geomorphic units such as floodplains, pediplain, and valley fills that cover most of the basin are appropriate for groundwater recharge. The impact of LULC on GWPZs assessment can be attributed to the fact that the bare land is favorable for recharge, and it occupies around 50% of the total basin area. The removal of rainfall alters GWPZs estimation due to the key role of the rainfall as being an important source of groundwater recharge. The removal of the lineaments influences the GWPZs assessment as lineaments enhance rocks' secondary porosity and permeability and thus increase the groundwater movement.

6. Conclusions

The present study demonstrated that remote sensing, GIS, and AHP approaches are feasible tools for demarcating GWPZs in the trans-boundary Shatt Al-Arab basin. The study provided a solid preliminary assessment for the groundwater resources in this basin in a more cost and time-effective way compared with the traditional techniques. Remote sensing data and conventional data were applied to compose the thematic layers that were then allocated appropriate weightage through the AHP technique. According to the GWPZs map, the study area is classified into five different zones, viz., a very good groundwater potential zone (12,136 km^2), good (66,578 km^2), moderate (51,836 km^2), poor (11,608 km^2), and very poor (953 km^2). Good GWPZ mapped in the southwestern areas of the basin are due to the favorable lithology (unconsolidated sediments), geomorphology units (floodplain and pediplain), and slope (flat terrains). On the other hand, poor GWPZs that cover the eastern parts of the study area can be ascribed to the accumulated influence of poor hydrogeological-environmental parameters (e.g., hilly and hard rock region). Sensitivity analysis has been conducted for each influencing factor to determine the most influencing factors for the GWPZs delineation. The most influencing factors here were lithology, geomorphology units, LULC, rainfall, and lineament density. The GWPZs map was compared with the wells' data (depth to groundwater) to approve its efficiency. We observed that the map is in agreement with the wells' observation data. The map prepared can be used as an initial step for positioning favorable locations of new productive wells in the Shatt Al-Arab basin without involving significant expenses. The technique of integrating remote sensing data and knowledge for accurate GWP evaluation applied in the current study gives scope for further research in groundwater exploration in this area. This approach is most appropriate for developing countries where comprehensive hydrogeological data are commonly unavailable. Moreover, this approach is in the direction of developing policies and future strategies for GWP monitoring at regular intervals for balancing the withdrawal and recharge capacities of aquifers to ensure sustainable groundwater resources usage in this water-stressed region.

Supplementary Materials: The following are available online at https://www.mdpi.com/2072-4292/13/1/112/s1, Figure S1: Digital Elevation Model (DEM) of the study area, Figure S2: Lithology of the study area, Figure S3: Annual rainfall of the study area, Figure S4: Geomorphology of the study area, Figure S5: Slope of the study area, Figure S6: Drainage density of the study area, Figure S7: Distance to rivers of the study area, Figure S8: Soils (dominant grain sizes) of the study area, Figure S9: LULC of the study area, Figure S10: Lineament density of the study area, Table S1: Accuracy assessment of GWPZs map with average groundwater water level.

Author Contributions: Conceptualization by H.A. and C.O.; Methodology, software, validation, and formal analysis by H.A., C.O., and S.P.; Investigation, data curation, and writing—original draft preparation by H.A. and C.O.; Supervision by C.O. All authors have read and agreed to the published version of the manuscript.

Funding: This research was funded by [Deutscher Akademischer Austauschdienst (DAAD)] grant number [57381412] and the APC was funded by [Philipps-University of Marburg].

Data Availability Statement: Data is contained within the article/supplementary material.

Acknowledgments: This research is part of PhD thesis of Hadi Allafta that is funded by the Deutscher Akademischer Austauschdienst (DAAD) [57381412].

Conflicts of Interest: The authors declare no conflict of interest.

References

1. Heyns, P. Water conservation in arid and semi-arid regions. *Water Resources Management—Vol. I.* Saveniji, H.H.G., Hoekstra, A.Y., Eds.; Encyclopedia of Life Support Systems (EOLSS)/UNESCO, 2009. Available online: https://www.eolss.net/ebooklib/bookinfo/water-resources-management.aspx# (accessed on 30 December 2020).
2. Singh, P.; Thakur, J.; Kumar, S. Delineating groundwater potential zones in a hardrock terrain using geospatial tools. *Hydrol. Sci. J.* **2013**, *58*, 213–223. [CrossRef]
3. Kahil, M.; Dinar, A.; Albiac, J. Modeling water scarcity and droughts for policy adaptation to climate change in arid and semiarid regions. *J. Hydrol.* **2015**, *522*, 95–109. [CrossRef]
4. Opp, C.; Wagemann, J.; Banadjschafie, S.; Abbasi, H. Aral Sea Syndrome and Lake Urmia crisis—A comparison of causes, effects and strategies for problem solutions. In *Geoparks and Geo-Tourism in Iran*; Dittmann, A., Ed.; Schriften zur Internationalen Entwicklungs- und Umweltforschung; PL Academic Research: Frankfurt, Germany; Bern, Switzerland; Brussels, Belgium; New York, NY, USA; Oxford, UK; Warszawa, Poland; Wien, Austria, 2017; Volume 34, pp. 169–183.
5. Li, P.; He, S.; Yang, N.; Xiang, G. Groundwater quality assessment for domestic and agricultural purposes in Yan'an City, Northwest China: Implications to sustainable groundwater quality management on the Loess Plateau. *Environ. Earth Sci.* **2018**, *77*, 775. [CrossRef]
6. Li, P.; Qian, H.; Wu, J. Conjunctive use of groundwater and surface water to reduce soil salinization in the Yinchuan Plain, North-West China. *Int. J. Water Resour. Dev.* **2018**, *34*, 337–353. [CrossRef]
7. Scott, K. Can The Middle East Solve Its Water Problem? Available online: https://edition.cnn.com/2018/07/11/middleeast/middle-east-water/index.html (accessed on 6 December 2020).
8. Michel, D. Iran's Impending Water Crisis. Water, Security and US Foreign Policy. In *Water, Security and US Foreign Policy*; Reed, D., Ed.; Routledge: New York, NY, USA, 2017; pp. 168–188.
9. Alkhafaji, H. Iraq's Water Crisis Challenges and Solutions. Al-Bayan Center for Planning and Studies. Available online: http://www.bayancenter.org/en/wp-content/uploads/2018/01/980987665.pdf (accessed on 6 December 2020).
10. UNESCO & EU Launching The Second Module of Capacity Building Support For The National Water Sector Of Iraq [EN/AR]—Iraq. Available online: https://reliefweb.int/report/iraq/unesco-eu-launching-second-module-capacity-building-support-national-water-sector-iraq (accessed on 6 December 2020).
11. Nabavi, E. Failed policies, falling aquifers: Unpacking groundwater overabstraction in Iran. *Water Altern.* **2018**, *11*, 699–724.
12. Abdullah, A.; Masih, I.; van der Zaag, P.; Karim, U.; Popescu, I.; Al Suhail, Q. Shatt al Arab River system under escalating pressure: A preliminary exploration of the issues and options for mitigation. *Int. J. River Basin Manag.* **2015**, *13*, 215–227. [CrossRef]
13. Al-Tawash, B.; Al-Lafta, H.; Merkel, B. Preliminary Assessment of Shatt Al-Arab Riverine Environment, Basra Governorate, Southern Iraq. *J. Nat. Sci. Res.* **2013**, *3*, 120–136.
14. Al-Saad, H.; Salman, N. Status of Oil Pollution in the Arabian Gulf and Shatt Al-Arab Estuary: A Review. In *Coastal Environments: Focus on Asian Regions*; Subramanian, V., Ed.; Springer: Dordrecht, The Netherlands, 2012. [CrossRef]
15. Moyel, M.; Hussain, N. Water quality assessment of the Shatt al-Arab River, Southern Iraq. *J. Coast. Life Med.* **2015**, *3*, 459–465.
16. Mahdi, B. Environmental pollution in Shatt Al-Arab estuary. *J. Int. Acad. Res. Multidiscip.* **2015**, *3*, 32–42.
17. Al-Saedi, A.; Smith, M.; Moles, N.; Alwhaely, U. Implications of Human Activities on the Shatt al Arab River and Khor al Zubair in City of Basra, Southern Iraq. In Proceedings of the 20th EGU General Assembly, EGU2018, Vienna, Austria, 8–13 April 2018; p. 17773.

18. Maltby, E. *An Environmental and Ecological Study of the Marshlands of Mesopotamia: Draft Consultive Bulletin*; AMAR Appeals Trust: London, UK, 1994.
19. Richardson, C.; Reiss, P.; Hussain, N.; Alwash, A.; Pool, D. The Restoration Potential of the Mesopotamian Marshes of Iraq. *Science* **2005**, *307*, 1307–1311. [CrossRef]
20. Al-Gburi, H.; Al-Tawash, B.; Al-Lafta, H. Environmental assessment of Al-Hammar Marsh, Southern Iraq. *Heliyon* **2017**, *3*, e00256. [CrossRef] [PubMed]
21. Abdullah, A.; Karim, U.; Masih, I.; Popescu, I.; Van der Zaag, P. Anthropogenic and tidal influences on salinity levels of the Shatt al-Arab River, Basra, Iraq. *Int. J. River Basin Manag.* **2016**, *14*, 357–366. [CrossRef]
22. Al-Yamani, F. Importance of the freshwater influx from the Shatt-Al-Arab River on the Gulf marine environment. In *Protecting the Gulf's Marine Ecosystems from Pollution*; Abuzinada, A.H., Barth, H.J., Krupp, F., Böer, B., Al Abdessalaam, T.Z., Eds.; Birkhäuser: Basel, Switzerland, 2008. [CrossRef]
23. Motagh, M.; Walter, T.; Sharifi, M.; Fielding, E. Land subsidence in Iran caused by widespread water reservoir overexploitation. *Geophys. Res. Lett.* **2008**, *35*, L16403. [CrossRef]
24. Abdullah, T.; Ali, S.; Al-Ansari, N.; Knutsson, S. Hydrogeochemical Evaluation of Groundwater and Its Suitability for Domestic Uses in Halabja Saidsadiq Basin, Iraq. *Water* **2019**, *11*, 690. [CrossRef]
25. Lashkaripour, G.; Ghafoor, M. The Effects of Water Table Decline on the Groundwater Quality in Aquifer of Torbat Jam Plain, Northeast Iran. *Int. J. Emerg. Sci.* **2011**, *1*, 153–163.
26. Al-Azawi, A.; Ward, F. Groundwater use and policy options for sustainable management in Southern Iraq. *Int. J. Water Resour. Dev.* **2016**, *33*, 628–648. [CrossRef]
27. Voss, K.; Famiglietti, J.; Lo, M.; De Linage, C.; Rodell, M.; Swenson, S. Groundwater depletion in the Middle East from GRACE with implications for transboundary water management in the Tigris-Euphrates-Western Iran region. *Water Resour. Res.* **2013**, *49*, 904–914. [CrossRef]
28. Al-Abadi, A.; Ghlaib, H.; Shahid, S. Flowing well potential zoning at Iraqi southern and western deserts using frequency ratio and geographic information system. *Int. J. Environ. Sci. Technol.* **2017**, *14*, 2249–2268. [CrossRef]
29. Ozdemir, A. Using a binary logistic regression method and GIS for evaluating and mapping the gorundwarer spring potential in the Sultan Mountians (Aksehir, Turkey). *J. Hydrol.* **2011**, *405*, 123–136. [CrossRef]
30. Etikala, B.; Golla, V.; Li, P.; Renati, S. Deciphering groundwater potential zones using MIF technique and GIS: A study from Tirupati area, Chittoor District, Andhra Pradesh, India. *HydroResearch* **2019**, *1*, 1–7. [CrossRef]
31. Anbazhagan, S.; Jothibasu, A. Geoinformatics in groundwater potential mapping and sustainable development: A case study from southern India. *Hydrol. Sci. J.* **2016**, *61*, 1109–1123. [CrossRef]
32. Battaglin, W.; Ltay, L.; Parker, R.; Leavesley, G. Applications of a gis for modeling the sensitivity of water resources to alternations in climate in the gunnisan river basin, Colorado. *Water Resour. Bull. Am. Water Res. Assoc.* **1993**, *25*, 1021–1028. [CrossRef]
33. Saraf, A.K. *A Report on Landscape Modelling in Gis for Bankura District, Project Sponsored by DST*; NRDMS division Government of India: New Delhi, Delhi, India, 1999.
34. Das, D.; Behara, S.C.; Kar, A.; Narendra, P.; Guha, S. Hydrogeomorphological mapping in groundwater exploration using remotely sensed data—A case study in Keonjhar District, Orissa. *J. Indian Soc. Remote Sens.* **1997**, *25*, 247–259. [CrossRef]
35. Ravindran, K.V.; Jeyaram, A. Groundwater prospects of Shahbad Tehsil, basan district, eastern Rajasthan. A remote sensing approach. *J. Indian Soc. Remote Sens.* **1997**, *25*, 239–246. [CrossRef]
36. Srinivas Rao, Y.; Reddy, T.; Nayudu, P. Groundwater targeting in hard rock terrain using fracture battern modelling, Niva river basin, Andhra Pradesh, India. *Hydrogeol. J.* **2000**, *8*, 494–502.
37. Sree Devi, P.D.; Srinivasalu, S.; Kesava Raju, K. Hydrogeomorphological and groundwater prospects of the Peregu river basin by using remote sensing data. *Environ. Geol.* **2001**, *40*, 1088–1094. [CrossRef]
38. Gopinath, G.; Saralathan, P. Identification of groundwater prospective zones using IRS-1D LISS and pump test methods. *J. Indian Soc. Remote Sens.* **2004**, *32*, 329–342. [CrossRef]
39. Kuria, D.; Gachari, M.; Macharia, M.; Mungai, E. Mapping groundwater potential in Kitui District, Kenyausing geospatial technologies. *Int. J. Water Res. Environ. Eng.* **2012**, *4*, 15–22.
40. Lillesand, T.M.; Kiefer, R.W.; Chipman, J. *Remote Sensing and Image Interpretation*; Wiley: New York, NY, USA, 2000.
41. Murthy, K. Groundwater potential in a semi-arid region of Andhra Pradeshda geographical information system approach. *Int. J. Remote Sens.* **2000**, *21*, 1867–1884. [CrossRef]
42. Solomon, S. Groundwater study using remote sensing and geographic information systems (GIS) in the central highlands of Eritrea. *Hydrogeol. J.* **2006**, *29*, 1034–1041.
43. Chowdhury, A.; Jha, M.; Chowdary, V.; Mal, B. Integrated remote sensing and GIS-based approach for assessing groundwater potential in West Medinipur district, West Bengal, India. *Int. J. Remote Sens.* **2009**, *30*, 231–250. [CrossRef]
44. Murugesan, B.; Thirunavukkarasu, R.; Senapathi, V.; Balasubramanian, G. Application of remote sensing and GIS analysis for groundwater potential zone in Kodaikanal Taluka, South India. *Front. Earth Sci.* **2012**, *7*, 65–75.
45. Elbeih, S. An overview of integrated remote sensing and GIS for groundwater mapping in Egypt. *Ain Shams Eng. J.* **2014**, *6*, 1–15. [CrossRef]
46. Sar, N.; Khan, A.; Chatterjee, S.; Das, A. Hydrologic delineation of ground water potential zones using geospatial technique for Keleghai river basin, India. *Model. Earth Syst. Environ.* **2015**, *1*, 25. [CrossRef]

47. Selvam, S.; Magesh, N.; Chidambaram, S.; Rajamanickam, M.; Sashikkumar, M. A GIS based identification of groundwater recharge potential zones using RS and IF technique: A case study in Ottapidaram taluk, Tuticorin district, Tamil Nadu. *Environ. Earth Sci.* **2015**, *73*, 3785–3799. [CrossRef]
48. Jothibasu, A.; Anbazhagan, S. Spatial mapping of groundwater potential in Ponnaiyar River basin using probabilistic-based frequency ratio model. *Model. Earth Syst. Environ.* **2017**, *3*, 33. [CrossRef]
49. Dar, I.; Sankar, K.; Dar, M. Deciphering groundwater potential zones in hard rock terrain using geospatial technology. *Environ. Monit. Assess.* **2011**, *173*, 597–610. [CrossRef]
50. Hutti, B.; Nijagunappa, R. Identification of groundwater potential zone using Geoinformatics in Ghataprabha basin, North Karnataka, India. *Int. J. Geomat. Geosci.* **2011**, *2*, 91–109.
51. Magesh, N.; Chandrasekar, N.; Soundranayagam, J. Delineation of groundwater potential zones in Theni district, Tamil Nadu, using remote sensing, GIS and MIF techniques. *Geosci. Front.* **2012**, *3*, 189–196. [CrossRef]
52. Mukherjee, P.; Singh, C.; Mukherjee, S. Delineation of groundwater potential zones in arid region of India—A remote sensing and GIS approach. *Water Resour. Manag.* **2012**, *26*, 2643–2672. [CrossRef]
53. Agarwal, E.; Agarwal, R.; Garg, R.; Garg, P. Delineation of groundwater potential zone: An AHP/ANP approach. *J. Earth Syst. Sci.* **2013**, *122*, 887–898. [CrossRef]
54. Awawdeh, M.; Obeidat, M.; Al-Mohammad, M.; Al-Qudah, K.; Jaradat, R. Integrated GIS and remote sensing for mapping groundwater potentiality in the Tulul al Ashaqif, Northeast Jordan. *Arab. J. Geosci.* **2013**, *7*, 2377–2392. [CrossRef]
55. Fashae, O.; Tijani, M.; Talabi, A.; Adedeji, O. Delineation of groundwater potential zones in the crystalline basement terrain of SW-Nigeria: An integrated GIS and remote sensing approach. *Appl. Water Sci.* **2014**, *4*, 19–38. [CrossRef]
56. Kaliraj, S.; Chandrasekar, N.; Magesh, N. Identification of potential groundwater recharge zones in Vaigai upper basin, Tamil Nadu, using GIS-based analytical hierarchical process (AHP) technique. *Arab. J. Geosci.* **2014**, *7*, 1385–1401. [CrossRef]
57. Kumar, T.; Gautam, A.; Kumar, T. Appraising the accuracy of GIS-based multi-criteria decision-making technique for delineation of groundwater potential zones. *Water Resour. Manag.* **2014**, *28*, 4449–4466. [CrossRef]
58. Ghosh, P.; Bandyopadhyay, S.; Jana, N. Mapping of groundwater potential zones in hard rock terrain using geoinformatics: A case of Kumari watershed in western part of West Bengal. *Model. Earth Syst. Environ.* **2016**, *2*, 1. [CrossRef]
59. Hussein, A.; Govindu, V.; Nigusse, A. Evaluation of groundwater potential using geospatial techniques. *Appl. Water Sci.* **2017**, *7*, 2447–2461. [CrossRef]
60. Yeh, H.; Cheng, Y.; Lin, H.; Lee, C. Mapping Groundwater Recharge Potential Zone Using a GIS Approach in Hualian River, Taiwan. *Sustain. Environ. Res.* **2016**, *26*, 33–43. [CrossRef]
61. Maity, D.; Mandal, S. Identification of groundwater potential zones of the Kumari river basin, India: An RS & GIS based semi-quantitative approach. *Environ. Dev. Sustain.* **2017**, *21*, 1013–1034. [CrossRef]
62. Pinto, D.; Shrestha, S.; Babel, M.; Ninsawat, S. Delineation of groundwater potential zones in the Comoro watershed, Timor Leste using GIS, remote sensing and analytic hierarchy process (AHP) technique. *Appl. Water Sci.* **2017**, *7*, 503–519. [CrossRef]
63. Das, B.; Pal, S.; Malik, S.; Chakrabortty, R. Modeling groundwater potential zones of Puruliya district, West Bengal, India using remote sensing and GIS techniques. *Geol. Ecol. Landsc.* **2018**, *3*, 223–237. [CrossRef]
64. Gnanachandrasamy, G.; Yongzhang, Z.; Bagyaraj, M.; Venkatramanan, S.; Ramkumar, T.; Shugong, W. Remote Sensing and GIS Based Groundwater Potential Zone Mapping in Ariyalur District, Tamil Nadu. *J. Geol. Soc. India* **2018**, *92*, 484–490. [CrossRef]
65. Lakshmi, S.; Reddy, Y. Identification of groundwater potential zones using GIS and remote sensing. *Int. J. Pure Appl. Math.* **2018**, *119*, 3195–3210.
66. Nasir, M.; Khan, S.; Zahid, H.; Khan, A. Delineation of groundwater potential zones using GIS and multi influence factor (MIF) techniques: A study of district Swat, Khyber Pakhtunkhwa, Pakistan. *Environ. Earth Sci.* **2018**, *77*, 367. [CrossRef]
67. Patra, S.; Mishra, P.; Mahapatra, S. Delineation of groundwater potential zone for sustainable development: A case study from Ganga Alluvial Plain covering Hooghly district of India using remote sensing, geographic information system and analytic hierarchy process. *J. Clean. Prod.* **2018**, *172*, 2485–2502. [CrossRef]
68. Arulbalaji, P.; Padmalal, D.; Sreelash, K. GIS and AHP Techniques Based Delineation of Groundwater Potential Zones: A case study from Southern Western Ghats, India. *Sci. Rep.* **2019**, *9*, 2082. [CrossRef]
69. Choubin, B.; Rahmati, O.; Soleimani, F.; Alilou, H.; Moradi, E.; Alamdari, N. Regional Groundwater Potential Analysis Using Classification and Regression Trees. In *Spatial Modeling in GIS and R for Earth and Environmental Sciences*, 1st ed.; Pourghasemi, H.R., Gokceoglu, C., Eds.; Elsevier: Amsterdam, The Netherlands, 2019; pp. 485–498. [CrossRef]
70. Kanagaraj, G.; Suganthi, S.; Elango, L.; Magesh, N. Assessment of groundwater potential zones in Vellore district, Tamil Nadu, India using geospatial techniques. *Earth Sci. Inf.* **2019**, *12*, 211–223. [CrossRef]
71. Raju, R.; Raju, G.; Rajasekhar, M. Identification of groundwater potential zones in Mandavi River basin, Andhra Pradesh, India using remote sensing, GIS and MIF techniques. *HydroResearch* **2019**, *2*, 1–11. [CrossRef]
72. Arshad, A.; Zhang, Z.; Zhang, W.; Dilawar, A. Mapping favorable groundwater potential recharge zones using a GIS-based analytical hierarchical process and probability frequency ratio model: A case study from an agro-urban region of Pakistan. *Geosci. Front.* **2020**. [CrossRef]
73. Benjmel, K.; Amraoui, F.; Boutaleb, S.; Ouchchen, M.; Tahiri, A.; Touab, A. Mapping of Groundwater Potential Zones in Crystalline Terrain Using Remote Sensing, GIS Techniques, and Multicriteria Data Analysis (Case of the Ighrem Region, Western Anti-Atlas, Morocco). *Water* **2020**, *12*, 471. [CrossRef]

74. Dar, T.; Rai, N.; Bhat, A. Delineation of potential groundwater recharge zones using analytical hierarchy process (AHP). *Geol. Ecol. Landsc.* **2020**. [CrossRef]
75. Kolli, M.; Opp, C.; Groll, M. Mapping of potential groundwater recharge zones in the Kolleru Lake catchment, India, by using remote sensing and GIS techniques. *Nat. Resour.* **2020**, *11*, 127–145. [CrossRef]
76. Kumar, V.; Mondal, N.; Ahmed, S. Identification of Groundwater Potential Zones Using RS, GIS and AHP Techniques: A Case Study in a Part of Deccan Volcanic Province (DVP), Maharashtra, India. *J. Indian Soc. Remote Sens.* **2020**, *48*, 497–511. [CrossRef]
77. Selvarani, A.G.; Elangovan, K.; Kumar, C. Evaluation of groundwater potential zones using electrical resistivity and GIS in Noyyal River basin, Tamil Nadu. *J. Geol. Soc. India* **2016**, *87*, 573–582. [CrossRef]
78. Machiwal, D.; Madan, K.; Jha, M.; Bimal, C.; Mal, B. Assessment of groundwater potential in a semi-arid region of India using remote sensing, GIS and MCDM techniques. *Water Resour. Manag.* **2011**, *25*, 1359–1386. [CrossRef]
79. Falah, F.; Ghorbani Nejad, S.; Rahmati, O.; Daneshfar, M.; Zeinivand, H. Applicability of generalized additive model in groundwater potential modelling and comparison its performance by bivariate statistical methods. *Geocarto Int.* **2017**, *32*, 1069–1089. [CrossRef]
80. Sashikkumar, M.; Selvam, S.; Kalyanasundaram, V.; Johnny, J. GIS based groundwater modeling study to assess the effect of artificial recharge: A case study from Kodaganar river basin, Dindigul district, Tamil Nadu. *J. Geol. Soc. India* **2017**, *89*, 57–64. [CrossRef]
81. Saranya, T.; Saravanan, S. Groundwater potential zone mapping using analytical hierarchy process (AHP) and GIS for Kancheepuram District, Tamilnadu, India. *Model. Earth Syst. Environ.* **2020**, *6*, 1105–1122. [CrossRef]
82. Saaty, T. Group decision making and the AHP. In *The Analytic Hierarchy Process*; Golden, B.L., Wasil, E.A., Harker, P.T., Eds.; Springer: Berlin/Heidelberg, Germany, 1980.
83. Saaty, T. *The Analytic Hierarchy Process*, 12th ed.; McGraw-Hill International Book Co.: New York, NY, USA, 1980.
84. Saaty, T. *Decision Making for Leaders: The Analytic Hierarchy Process for Decisions in a Complex World*; RWS Publications: Pittsburgh, PA, USA, 2014.
85. Brunelli, M. *Introduction to the Analytic Hierarchy Process*; Springer: New York, NY, USA, 2015.
86. Souissi, D.; Msaddek, M.; Zouhri, L.; Chenini, I.; El May, M.; Dlala, M. Mapping groundwater recharge potential zones in arid region using GIS and Landsat approaches, southeast Tunisia. *Hydrol. Sci. J.* **2018**, *63*, 251–268. [CrossRef]
87. Rahaman, S.; Ajeez, S.; Aruchamy, S.; Jegankumar, R. Prioritization of Sub Watershed Based on Morphometric Characteristics Using Fuzzy Analytical Hierarchy Process and Geographical Information System—A Study of Kallar Watershed, Tamil Nadu. *Aquat. Procedia* **2015**, *4*, 1322–1330. [CrossRef]
88. Bisson, R.; Lehr, J. Sudan Case Studies and Model. In *Modern Groundwater Exploration*; Bisson, R.A., Lehr, J.H., Eds.; John Wiley & Sons: Hoboken, NJ, USA, 2014.
89. Naghibi, S.; Pourghasemi, H.; Pourtaghi, Z.; Rezaei, A. Groundwater qanat potential mapping using frequency ratio and Shannon's entropy models in the Moghan watershed, Iran. *Earth Sci. Inf.* **2015**, *8*, 171–186. [CrossRef]
90. Mallick, J.; Khan, R.; Ahmed, M.; Alqadhi, S.; Alsubih, M.; Falqi, I.; Abul Hasan, M. Modeling Groundwater Potential Zone in a Semi-Arid Region of Aseer Using Fuzzy-AHP and Geoinformation Techniques. *Water* **2019**, *11*, 2656. [CrossRef]
91. Malczewski, J. GIS-based multicriteria decision analysis: A survey of the literature. *Int. J. Geogr. Inf. Sci.* **2006**, *20*, 703–726. [CrossRef]
92. UN-ESCWA and BGR (United Nations Economic and Social Commission for Western Asia; Bundesanstalt für Geowissenschaften und Rohstoffe). Inventory of Shared Water Resources in Western Asia. Beirut. Available online: https://waterinventory.org/sites/waterinventory.org/files/chapters/Chapter-05-Shatt-al-Arab-Karkheh-and-Karun-Rivers-web_0.pdf (accessed on 6 December 2020).
93. Buday, T.; Jassim, S. *Final Report and the Regional Geological Survey of Iraq*; Unpub. Report SOM; Library Tectonic Framework: Baghdad, Iraq, 1984; Volume 2.
94. Aqrawi, A.; Goff, J.; Horbury, A.; Sadooni, F. *The Petroleum Geology of Iraq*; Scientific Press Ltd.: Beaconsfield, UK, 2010; 424p.
95. Al-Musawi, F.; Idan, R.; Salih, A. Reservoir Properties and Facies Distribution of Mishrif Formation in Ratawi Oilfield, Southern Iraq. In *The Structural Geology Contribution to the Africa-Eurasia Geology: Basement and Reservoir Structure, Ore Mineralisation and Tectonic Modelling*; Rossetti, F., Blanc, A.C., Riguzzi, F., Leroux, E., Pavlopoulos, K., Bellier, O., Kapsimalis, V., Eds.; Advances in Science, Technology & Innovation (IEREK Interdisciplinary Series for Sustainable Development); Springer: Cham, Switzerland, 2019. [CrossRef]
96. Idan, R.; Al-Musawi, F.; Salih, A.; Al-Qaraghuli, S. The Petroleum System of Zubair Formation in Zubair Subzone, Southern Iraq. *J. Pet. Res. Stud.* **2019**, *25*, E57–E73.
97. Berberian, M.; King, G. Towards the paleogeography and tectonic evolution of Iran. *Can. J. Earth Sci.* **1981**, *18*, 210–265. [CrossRef]
98. Issar, I. The groundwater provinces of Iran. *Bull. Int. Assoc. Sci. Hydrol.* **1969**, *14*, 87–99. [CrossRef]
99. Country Data Info. Available online: https://www.laenderdaten.info/ (accessed on 6 December 2020).
100. Riad, P.; Billib, M.; Hassan, A.; Salam, M.A.; El Din, M.N. Application of the overlay weighted model and boolean logic to determine the best locations for artificial recharge of groundwater. *J. Urban Environ. Eng.* **2011**, *5*, 57–66. [CrossRef]
101. Lentswe, G.; Molwalefhe, L. Delineation of potential groundwater recharge zones using analytic hierarchy process-guided GIS in the semi-arid Motloutse watershed, eastern Botswana. *J. Hydrol. Reg. Stud.* **2020**, *28*, 100674. [CrossRef]

102. Selvam, S.; Farooq, A.; Magesh, N.; Singaraja, C.; Venkatramanan, S.; Chung, S. Application of remote sensing and GIS for delineating groundwater recharge potential zones of Kovilpatti Municipality, Tamil Nadu using IF technique. *Earth Sci. Inf.* **2016**, *9*, 137–150. [CrossRef]
103. Tolche, A. Groundwater potential mapping using geospatial techniques: A case study of Dhungeta-Ramis sub-basin, Ethiopia. *Geol. Ecol. Landsc.* **2020**. [CrossRef]
104. Rahmati, O.; Samani, A.; Mahdavi, M.; Pourghasemi, H.; Zeinivand, H. Groundwater potential mapping at Kurdistan region of Iran using the analytic hierarchy process and GIS. *Arab. J. Geosci.* **2015**, *8*, 7059–7071. [CrossRef]
105. Waikar, M.; Nilawar, A. Identification of Groundwater Potential Zone using Remote Sensing and GIS Technique. *Int. J. Innov. Res. Sci. Eng. Technol.* **2014**, *3*, 12163–12174.
106. Al Saud, M. Mapping potential areas for groundwater storage in Wadi Aurnah Basin, western Arabian Peninsula, using remote sensing and geographic information system techniques. *Hydrogeol. J.* **2018**, *18*, 1481–1495. [CrossRef]
107. Strahler, A. Quantitative Geomorphology of Drainage Basins and Channel Networks. In *Handbook of Applied Hydrology*; Chow, V., Ed.; McGraw Hill: New York, NY, USA, 1964; pp. 439–476.
108. Chowdhury, A.; Jha, M.; Chowdary, V. Delineation of groundwater recharge zones and identification of artificial recharge sites in West Medinipur district, West Bengal, using RS, GIS and MCDM techniques. *Environ. Earth Sci.* **2010**, *9*, 1209–1222. [CrossRef]
109. Opp, C. Bodenkörper. In *Geographie—Physische Geographie und Humangeographie*, 3rd ed.; Gebhardt, H., Glaser, R., Radtke, U., Reuber, P., Vött, A., Eds.; Springer: Berlin, Germany, 2011; pp. 485–490.
110. Saaty, T. Decision-making with the AHP: Why is the principal eigenvector necessary. *Eur. J. Oper. Res.* **2003**, *145*, 85–91. [CrossRef]
111. Goepel, K. Implementing the Analytic Hierarchy Process as a Standard Method for Multi-Criteria Decision Making in Corporate Enterprises—A New AHP Excel Template with Multiple Inputs. In Proceedings of the International Symposium on the Analytic Hierarchy Process, Kuala Lumpur, Malaysia, 23–26 June 2013. [CrossRef]
112. Machiwal, D.; Rangi, N.; Sharma, A. Integrated knowledge- and data-driven approaches for groundwater potential zoning using GIS and multi-criteria decision-making techniques on hard-rock terrain of Ahar catchment, Rajasthan, India. *Environ. Earth Sci.* **2015**, *73*, 1871–1892. [CrossRef]
113. Saaty, T. How to make a decision: The analytic hierarchy process? *Eur. J. Oper. Res.* **1990**, *48*, 9–26. [CrossRef]
114. Malczewski, J. *GIS and Multicriteria Decision Analysis*; Wiley: Hoboken, NJ, USA, 1999.
115. Shaban, A.; Khawlie, M.; Abdallah, C. Use of remote sensing and GIS to determine recharge potential zone: The case of Occidental Lebanon. *Hydrogeol. J.* **2006**, *14*, 433–443. [CrossRef]
116. El-Baz, F.; Himida, I. *Groundwater Potential of the Sinai Peninsula, Egypt*; Boston University: Boston, MA, USA, 1995.
117. Universität Hamburg. Available online: https://www.geo.uni-hamburg.de/geologie/forschung/geochemie/glim.html (accessed on 6 December 2020).
118. Gebhardt, H.; Glaser, R.; Radtke, U.; Reuber, P. (Eds.) *Geographie. Physische Geographie und Humangeographie*, 2nd ed.; Springer: Berlin/Heidelberg, Germany, 2011.
119. Krishnamurthy, J.; Srinivas, G. Role of geological and geomorphological factors in ground water exploration: A study using IRS LISS data. *Int. J. Remote Sens.* **1995**, *16*, 2595–2618. [CrossRef]
120. Suganthi, S.; Elango, L.; Subramanian, S. Groundwater potential zonation by Remote Sensing and GIS techniques and its relation to the Groundwater level in the Coastal part of the Arani and Koratalai River Basin, Southern India. *Earth Sci. Res. J.* **2013**, *17*, 87–95.
121. Gupta, M.; Srivastava, P. Integrating GIS and remote sensing for identification of groundwater potential zones in the hilly terrain of Pavagarh, Gujarat, India. *Water Int.* **2010**, *35*, 233–245. [CrossRef]
122. Satapathy, I.; Syed, T. Characterization of groundwater potential and artificial recharge sites in Bokaro District, Jharkhand (India), using remote sensing and GIS-based techniques. *Environ. Earth Sci.* **2015**, *74*, 4215–4232. [CrossRef]
123. Wooding, R. A hydraulic modelfor the catchment stream problem. III Comparison with runoff observations. *J. Hydrol.* **1966**, *4*, 21–37. [CrossRef]
124. Sener, E.; Davraz, A.; Ozcelik, M. An integration of GIS and remote sensing in groundwater investigations: A case study in Burdur, Turkey. *Hydrogeol. J.* **2005**, *13*, 826–834. [CrossRef]
125. Rajaveni, S.; Brindha, K.; Elango, L. Geological and geomorphological controls on groundwater occurrence in a hard rock region. *Appl. Water Sci.* **2015**, *7*, 1377–1389. [CrossRef]
126. Moghaddam, D.; Rezaei, M.; Pourghasemi, H.; Pourtaghie, Z.; Pradhan, B. Groundwater spring potential mapping using bivariate statistical model and GIS in the Taleghan Watershed, Iran. *Arab. J. Geosci.* **2015**, *8*, 913–929. [CrossRef]
127. Anbazhagan, S.; Ramasamy, S.; Das Gupta, S. Remote sensing and GIS for artificial recharge study, runoff estimation and planning in Ayyar basin, Tamil Nadu, India. *Environ. Geol.* **2005**, *48*, 158–170. [CrossRef]
128. Scanlon, B.; Reedy, R.; Stonestrom, D.; Prudic, D.; Dennehy, K. Impact of land use and land cover change on groundwater recharge and quality in the southwestern US. *Glob. Chang. Biol.* **2005**, *11*, 1577–1593. [CrossRef]
129. USGS. Available online: https://www.usgs.gov/special-topic/water-science-school/science/infiltration-and-water-cycle?qt-science_center_objects=0#qt-science_center_objects (accessed on 6 December 2020).
130. Enderle, D.; Weih, R. Integrating supervised and unsupervised classification methods to develop a more accurate land cover classification. *J. Ark. Acad. Sci.* **2005**, *59*, 65–73. Available online: http://scholarworks.uark.edu/jaas/vol59/iss1/10 (accessed on 6 December 2020).

131. O'Leary, D.; Friedman, J.; Pohn, H. Lineament, linear, lineation: Some proposed new standards for old terms. *Geol. Soc. Am. Bull.* **1976**, *87*, 1463–1469. [CrossRef]
132. Bahiru, E.; Woldai, T. Integrated geological mapping approach and gold mineralization in Buhweju area, Uganda. *Ore Geol. Rev.* **2016**, *72*, 777–793. [CrossRef]
133. Saepuloh, A.; Haeruddin, H.; Heriawan, M.; Kubo, T.; Koike, K.; Malik, D. Application of lineament density extracted from dual orbit of synthetic aperture radar (SAR) images to detecting fluids paths in the Wayang Windu geothermal field (West Java, Indonesia). *Geothermics* **2018**, *72*, 145–155. [CrossRef]
134. Krishna, R.; Kishan, D.; Sarup, J. Lineament extraction and lineament density assessment of Omkareshwar, M P, India, using GIS Techniques. *Int. J. Eng. Manag. Res.* **2015**, *5*, 717–720.
135. Soe, M.; Ryutaro, T.; Ishiyama, D.; Takashima, I.; Won-In, K.; Charusiri, P. Remote sensing and GIS based approach for earthquake probability map: A case study of the northern Sagaing fault area, Myanmar. *J. Geol. Soc. Thail.* **2009**, *1*, 29–46.
136. Muthumaniraja, C.K.; Anbazhagan, S.; Jothibasu, A.; Chinnamuthu, M. Remote Sensing and Fuzzy Logic Approach for Artificial Recharge Studies in Hard Rock Terrain of South India. In *GIS and Geostatistical Techniques for Groundwater Science*; Elsevier: Amsterdam, The Netherlands, 2019; pp. 91–112. [CrossRef]
137. Qari, M. Lineament extraction from multi-resolution satellite imagery: A pilot study on Wadi Bani Malik, Jeddah, Kingdom of Saudi Arabia. *Arab. J. Geosci.* **2011**, *4*, 1363–1371. [CrossRef]
138. Chitsazan, M.; Akhtari, Y. A GIS-based DRASTIC Model for Assessing Aquifer Vulnerability in Kherran Plain, Khuzestan, Iran. *Water Resour. Manag.* **2009**, *23*, 1137–1155. [CrossRef]
139. Khodabakhshi, N.; Asadollahfardi, G.; Heidarzadeh, N. Application of a GIS-based DRASTIC model and groundwater quality index method for evaluation of groundwater vulnerability: A case study, Sefid-Dasht. *Water Sci. Technol. Water Supply* **2015**, *15*, 784–792. [CrossRef]
140. Alkinani, M.; Kanoua, W.; Merkel, B. Uranium in groundwater of the Al-Batin Alluvial Fan aquifer, south Iraq. *Environ. Earth Sci.* **2016**, *75*, 869. [CrossRef]
141. Goumehei, E.; Geravandi, Y.; Yan, W. A GIS-Based Study to Investigate Effect of Water Table Changes on DRASTIC Model: A Case Study of Kermanshah, Iran. *Int. J. Environ. Geoinform.* **2016**, *3*, 76–82. [CrossRef]
142. Taheri, K.; Taheri, M.; Parise, M. Impact of intensive groundwater exploitation on an unprotected covered karst aquifer: A case study in Kermanshah Province, western Iran. *Environ. Earth Sci.* **2016**, *75*, 1221. [CrossRef]
143. Yousefi, H.; Haghizadeh, A.; Yarahmadi, Y.; Hasanpour, P.; Noormohamadi, P. Groundwater pollution potential evaluation in Khorramabad-Lorestan Plain, western Iran. *J. Afr. Earth. Sci.* **2018**, *147*, 647–656. [CrossRef]
144. Gogu, R.; Dassargues, A. Sensitivity analysis for the EPIK method of vulnerability assessment in a small karstic aquifer, southern Belgium. *Hydrogeol. J.* **2000**, *8*, 337–345. [CrossRef]
145. Pathak, D.; Hiratsuka, A.; Awata, I.; Chen, L. Groundwater vulnerability assessment in shallow aquifer of Kathmandu Valley using GIS-based DRASTIC model. *Environ. Geol.* **2009**, *57*, 1569–1578. [CrossRef]
146. Lodwick, W.A.; Monson, W.; Svoboda, L. Attribute error and sensitivity analysis of map operations in geographical information systems: Suitability analysis. *Int. J. Geogr. Inf. Sci.* **1990**, *4*, 413–428. [CrossRef]
147. Domas, J. *The Geology of Karbala–Kut–Ali Al-Gharbi Area*; GEOSURV: Baghdad, Iraq, 1985.
148. Earle, S. *Physical Geology*, 2nd ed.; BCcampus: Victoria, BC, Canada, 2019; Available online: https://opentextbc.ca/physicalgeology2ed/ (accessed on 6 December 2020).
149. Rekha, V.B.; Thomas, A.P.; Suma, M.; Vijith, H. An integration of spatial information technology for groundwater potential and quality investigations in Koduvan Ar Sub—Watershed of Meenachil River Basin, Kerala, India. *J. Indian Soc. Remote Sens.* **2011**, *39*, 63–71. [CrossRef]
150. Kotchoni, D.; Vouillamoz, J.; Lawson, F.; Adjomayi, P.; Boukari, M.; Taylor, R. Relationships between rainfall and groundwater recharge in seasonally humid Benin: A comparative analysis of long-term hydrographs in sedimentary and crystalline aquifers. *Hydrogeol. J.* **2019**, *27*, 447–457. [CrossRef]
151. Thapa, R.; Gupta, S.; Guin, S.; Kaur, H. Assessment of groundwater potential zones using multi-influencing factor (MIF) and GIS: A case study from Birbhum district, West Bengal. *Appl. Water Sci.* **2017**, *7*, 4117–4131. [CrossRef]
152. Sankar, K. Evaluation of Groundwater Potential Zones Using Remote Sensing Data In Upper Vaigai River Basin, Tamil Nadu, India. *J. Indian Soc. Remote Sens.* **2002**, *30*, 119–129. [CrossRef]
153. Sharma, D.; Jugran, D.K. Hydrogeomorphological Studies around PinjaurMomi-Kala Arab Area, Ambala District (Hariyana) and Sirmour District (Himachala Pradesh). *J. Indian Soc. Remote Sens.* **1992**, *20*, 187–197. [CrossRef]
154. Sparks, B. Landforms in arid and semi-arid climates. In *Geomorphology*, 2nd ed.; Longman Group Ltd.: London, UK, 1960; pp. 335–341.
155. Ramaiah, S.; Gopalakrishna, G.; Vittala, S.; Najeeb, K. Geomorphological mapping for identification of ground water potential zones in hard rock areas using geo-spatial information—A case study in Malur Taluk, Kolar District, Karnataka, India. *Nat. Environ. Pollut. Technol.* **2012**, *11*, 369–376.
156. Al-Djazouli, M.; Elmorabiti, K.; Rahimi, A.; Amellah, O.; Fadil, O. Delineating of groundwater potential zones based on remote sensing, GIS and analytical hierarchical process: A case of Waddai, eastern Chad. *GeoJournal* **2020**. [CrossRef]
157. Subba Rao, N. Groundwater potential index in a crystalline terrain using remote sensing data. *Environ. Geol.* **2006**, *50*, 1067–1076. [CrossRef]

158. Mogaji, K.; Omosuyi, G.; Adelusi, A.; Lim, H. Application of GIS-Based Evidential Belief Function Model to Regional Groundwater Recharge Potential Zones Mapping in Hardrock Geologic Terrain. *Environ. Process.* **2016**, *3*, 93–123. [CrossRef]
159. Razavi-Termeh, S.; Sadeghi-Niaraki, A.; Choi, S. Groundwater Potential Mapping Using an Integrated Ensemble of Three Bivariate Statistical Models with Random Forest and Logistic Model Tree Models. *Water* **2019**, *11*, 1596. [CrossRef]
160. Oh, H.; Kim, Y.; Choi, J.; Park, E.; Lee, S. GIS mapping of regional probabilistic groundwater potential in the area of Pohang City, Korea. *J. Hydrol.* **2011**, *399*, 158–172. [CrossRef]
161. Gee, G.; Fayer, M.; Rockhold, M.; Campbell, M. Variation in recharge at the Hanford site. *Northwest Sci.* **1992**, *66*, 237–250.
162. Brouwer, C.; Prins, K.; Kay, M.; Heibloem, M. *Irrigation Water Management: Irrigation Methods*; Training Manual No. 5. Food and Agriculture Organization of the United Nations, 1988. Available online: http://www.fao.org/3/S8684E/s8684e00.htm#Contents (accessed on 9 November 2020).
163. Owuor, S.; Butterbach-Bahl, K.; Guzha, A.; Rufino, M.; Pelster, D.; Díaz-Pinés, E.; Breuer, L. Groundwater recharge rates and surface runoff response to land use and land cover changes in semi-arid environments. *Ecol. Process.* **2016**, *5*, 16. [CrossRef]
164. Albhaisi, M.; Brendonck, L.; Batelaan, O. Predicted impacts of land use change on groundwater recharge of the upper Berg catchment, South Africa. *Water SA* **2013**, *39*, 2. [CrossRef]
165. Roark, D.; Healy, D. *Quantification of Deep Percolation from Two Flood-Irrigated Alfalfa Fields, Roswell Basin, New Mexico*; USGS Water Resources Investigation Report 98-4096; U.S. Department of the Interior, U.S. Geological Survey: Albuquerque, NM, USA, 1998; 32p. Available online: https://pubs.usgs.gov/wri/1998/4096/report.pdf (accessed on 30 December 2020).
166. Jat, M.; Khare, D.; Garg, P. Urbanization and its impact on groundwater: A remote sensing and GIS-based assessment approach. *Environmentalist* **2009**, *29*, 17–32. [CrossRef]
167. British Geological Survey. Available online: https://www.bgs.ac.uk/discoveringGeology/hazards/earthquakes/plateTectonics.html (accessed on 6 December 2020).
168. Saraf, A.; Choudhury, P. Integrated remote sensing and GIS for groundwater exploration and identification of artificial recharge sites. *Int. J. Remote Sens.* **1998**, *19*, 1825–1841. [CrossRef]
169. Raviraj, A.; Kuruppath, N.; Kannan, B. Identification of Potential Groundwater Recharge Zones Using Remote Sensing and Geographical Information System in Amaravathy Basin. *J. Remote Sens. GIS* **2017**, *6*, 213. [CrossRef]